1. Review #1

In this document, the reviewer comments are in black, the authors responses are in red.

The authors thank the reviewer for their thoughtful and productive comments.

SUMMARY: This paper discusses the analyses of wind turbine wake structure considering varying atmospheric stability regimes using measurements from a single scanning lidar; representing an extension of the work of Aiken and Lundquist (JTECH, 2014). Frequency in wake detection, wake velocity deficits, wake width, and wake centerline results are presented. I found the discussion related to the wake stretching as a result of vertically veering wind direction to particularly interesting. The impact of atmospheric stability on wake behavior is a very important aspect to understanding wind plant performance as a whole, and as this paper shows there are significant and consistent (e.g. diurnal) changes in wake behavior as a result of the background stability. I believe the results of this paper are a meaningful contribution and worthy of publication, but I do have a few comments/questions requesting clarity for how the measurements are used to construct the analyses and what the downstream implications are for the presented results.

Thank you for finding our work interesting and useful!

MAJOR COMMENTS/QUESTIONS: While the title infers a 3D construction of the wakes for analysis, in reality, all of the presented wake statistics are only assessed from individual 2D planes. Since multiple elevation tilts are used, I would have liked to see the author construct fully integrated 3D volumes of data by interpolating the polar data from a given elevation series (by elevation series I mean a single collection of the six elevation tilts between 1.5-2.8 degrees) into a 3D Cartesian grid. Otherwise, when assessing wake deficit and width, how can we be certain that any given 2D plane is a complete representation of the absolute downwind wake deficit or wake width since that plane only represents a horizontal 2D "slice" somewhere through the wake?

You are right: single 2D plans cannot be considered as a full representation of wake characteristics. In fact, we considered data from PPI scans performed at all the six elevation angles to retrieve results for the velocity deficit and the wake width. As shown in Figure 2, we can in this way produce a representation of a considerable part of the whole wake region, at different altitudes and different downwind distances from the turbine.

Since deficits and widths were computed separately from the individual PPI elevation planes within the same elevation series, this would mean multiple wake deficit/width calculations for the same downwind distance exist within the same elevation series, but inherently represent different vertical locations within the wake. Or maybe the generated wake statistics for one elevation series

are binned by range regardless of their height?

For the whole discussion of the velocity deficit and the wake width, all the different elevation angles of the PPI scans are included in the results: the focus for these two characteristics is mainly on how these change with downwind distance and how different relative position (i.e. inner vs outer wakes) affect the results.

Additional discussion on how the statistics from individual tilts within a single elevation series are merged (or not) would provide for a better understanding of the bulk wake statistics (e.g. deficit and width) and how representative the statistics are of the character of the full wake at any given downwind distance.

Thank you for noticing that our discussion about the different elevation angles was not clear. The revised manuscript will clearly state that all the six elevation angles are used to retrieve the results regarding wake width and velocity deficit: "during all the scans (at all the considered elevation angles) performed on 23 and 26 August 2013".

I apologize if I have misinterpreted the analysis, but I believe there needs to be further clarification of how the 2D planes of PPI data are used to generate the wake statistics, and what inherent assumptions/limitations are associated with the methods. I would also encourage the author, though not required, to consider analyzing the data in a true 3D framework when constructing the presented wake statistics.

Although we appreciate the suggestion of a full 3D framework retrieval of the wake structure, we think that the way we chose to present our results – now improved to better explain how we used different elevation angles – is more intuitive and similar to the presentation style of comparable results in the literature in this field (Aitken et al. 2014, Banta et al. 2015, among the others). Thus, we decided to keep our way to present the results; however, we thank the reviewer for their useful suggestion, which might be implemented in a future paper about the topic, possibly using data from different field campaigns.

MINOR COMMENTS/QUESTIONS:

1. P4, L8: What is the range from the WINDCUBE to the four turbines of interest? The distances can be inferred from Figure 2, but the numbers would be useful in the text.

The revised caption of Figure 2 will include the distances of the four considered turbines from the scanning lidar (2136 m, 2102 m, 2171 m, and 2286 m).

2. P 4, L 14: What is the scan speed of the lidar? What range of azimuths are scanned?

The scan speed of the lidar during a PPI scans was of 0.5deg/s. Each PPI scan spanned an azimuth range of 50deg. The revised manuscript will include the following sentence: "each PPI scan lasted approximately 100 seconds, spanning an azimuth range of 50 deg with a speed of 0.5 deg/s."

3. P4, L 19: How long does it take the lidar to scan the series of six elevation tilts?

The following table with a detailed description of the scan pattern – and its duration - used in the experiment will be included in the manuscript, along with an explicit statement that "Approximately ten minutes were required to collect the series of six elevation tilts":

Table 2. *Description of the 30-min cycle of scanning lidar scans in CWEX-13 field campaign. The characteristic fixed angle refers to the elevation angle for PPI and VAD scans, the azimuth angle for RHI scans.*

number of scans	type of scan	characteristic fixed angle	duration of each scan	cumulative time
2	VAD	75°, 60°	132 s	0:00 - 4:24
6	PPI	2.8°, 2.5°, 2.2°, 2.1°, 1.8°, 1.5°	104 s	4:24 - 14:48
3	RHI	160°, 170°, 180°	32 s	14:48 - 16:24
6	PPI	2.8°, 2.5°, 2.2°, 2.1°, 1.8°, 1.5°	104 s	16:24 - 26:48
6	RHI	160°, 170°, 180°, 180°, 170°, 160°	32 s	26:48 - 30:00

4. P9, L 11: This comment relates to the Major Comments/Questions section above. How is the ambient flow wind speed defined on the 2D PPI plane? Since the PPI plane is slanted, if the ambient flow wind speed is determined upstream of a given turbine, can you comment on the impact of using this value for constructing wake deficits downstream of the turbine, but at lower heights due to the slanted PPI plane? Is the comparison being made at different heights because the PPI plane is sloped? If so, what are the implications on the wake deficit calculations?

Thank you for pointing out that we did not specify which ambient flow speed we used for this calculation. The ambient flow wind speed is estimated (as one of the parameters of the used models) by our wake characterization algorithm at each range gate in each PPI scan. Thus, since we have a different value for each range gate, different vertical levels do not affect this calculation. To make this clear, we will rephrase the sentence as follows: "the ambient flow wind speed u (estimated from our algorithm at each performed fit at each range gate and elevation)".

5. P9, L30: How many scans are used to generate the statistics in Figure 5? Are all of the 438/576 scans performed on 23 Aug/26 Aug considered? Are all elevation tilts considered?

Yes, all the scans at all elevation angles are considered in this Figure. Thanks for pointing out that this had not been clearly stated in the text. The following sentence will be added to clarify this: "during all the 438/576 scans (at all the considered elevation angles) performed on 23/26 August

2013".

6. P10, L13: Does this statement imply that a single elevation series of six scans takes 11 minutes to complete? If so, that may answer Question 3 above.

Yes it does. However, as stated above, the duration of the scans will be explicitly shown in a table in the revised manuscript.

7. P10, L18: While the difference in wake deficit between the inner and outer wakes is shown, can the author comment on the difference in wake deficit between the outer turbines, as that difference is actually more substantial? Which line is for which turbine? Assuming the wind direction is relatively consistent throughout (maybe a bad assumption), can a composite PPI image be provided corresponding with this period to highlight if there are any features in the flow (e.g. a turbine row edge effect) that could be contributing?

See our answer to the next comment below.

8. P12, L2: While the author states comparable results occur between the 23-August and 26-August cases, do the red lines, for example, flip with the different wind direction, again inferring some type of turbine row edge effect?

Thank you for your thoughts about this result. We will change our Figure to label the individual turbines, as follows:

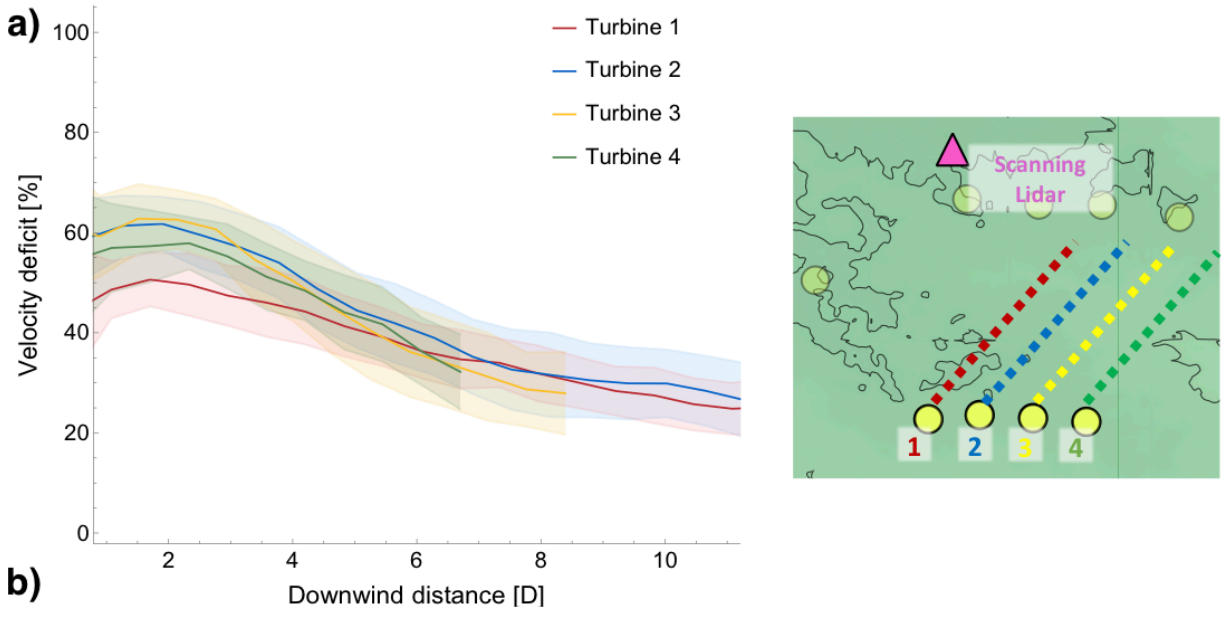

The sketch on the right will also help the reader to remember the wind direction for the considered

day.

Thank you also for pointing out that our comparison between 23 and 26 August was not clear enough. To solve this issue, we will include the plot for 23 August (see below) in Figure 7, whose caption will be rephrased as: "Velocity deficit vs downwind distance, for the four wakes of the studied row of turbines. Continuous lines represent the median values calculated from the PPI scans performed at all the considered elevation angles during the night (stable conditions) of 26 (panel a) and 23 (panel b) August 2013".

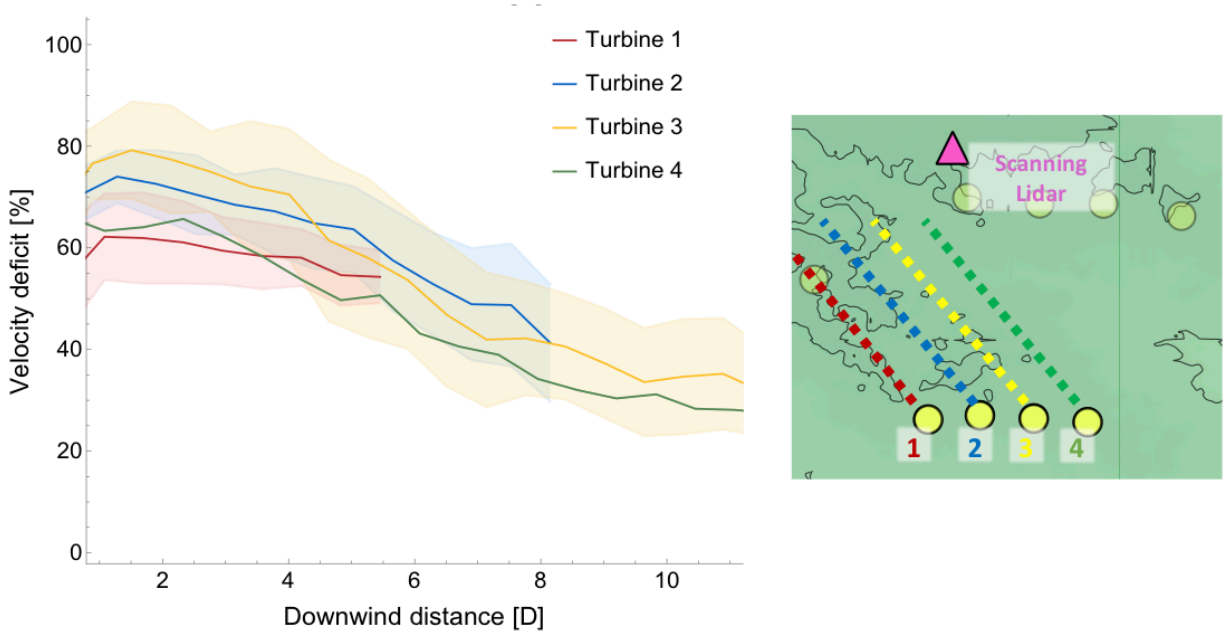

As can be seen, for the 23 August 2013 the difference between outer (turbines 1 and 4) and inner (turbines 2 and 3) wakes is more consistent for all the studied turbines, and the difference between the velocity deficit for the two outer turbines (noticed by the reviewer for the 26 August case) is not present anymore. Therefore, we cannot infer general results for other flow features (e.g. edge effects) beyond what we stated in the paragraph: "wakes from outer turbines (number 1 and number 4), have lower velocity deficits than the wakes from inner turbines (number 2 and number 3), for relatively small downwind distances, with a difference up to 15%".

9. P12, L18: Could an example PPI image or composite be included to visually highlight the wind direction dependence on wake width detection being discussed here?

This dependence can be seen in the following two color-maps of the line-of-sight velocity measured in two PPI scans during 23 and 26 August, which will be included in the manuscript at the end of the "Lidar measurements" section:

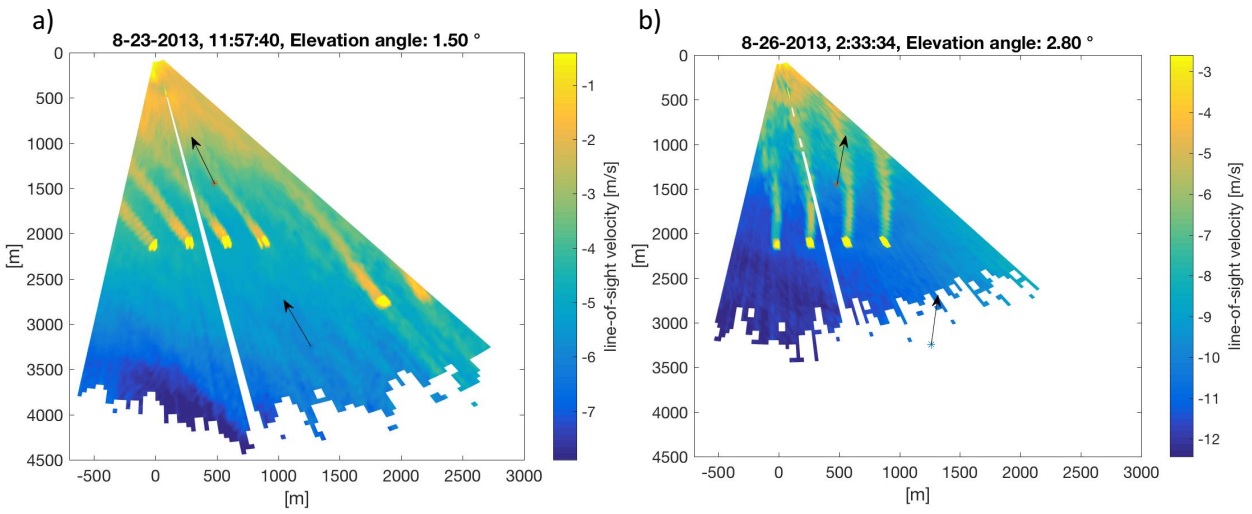

The caption of the Figure will be: "Figure 3. Color maps of line-of-sight velocity measured by the scanning lidar during two PPI scans performed at 11:57 UTC (6:57 am LDT) on 23 August 2013 (panel a) and at 02:33 UTC (9:33 pm LDT) on 26 August 2013 (panel b). The scanning lidar is located in the origin of the coordinate system. The two arrows show wind direction as measured by the profiling lidars WC-1 and WC-2 at 80 m AGL."

Moreover, we will add the following paragraph and Figure to better explain our interpretation of this result:

"This result is due to the relationship between the viewing angle and the aspect ratio of the lidar retrieval "pixels", which are related to the relatively long range gate (50 m) and relatively narrow azimuthal resolution (0.5 degree). As qualitatively shown in the schematic of Figure 10, the scanning lidar measures the line-of-sight velocity in narrow pencil-shaped "pixels". With this geometry, if the wind direction - and thus the wake - is aligned with the line-of-sight from the lidar, the wake width can be assessed with high precision due to the high azimuthal resolution in each pencil-shaped area (panel a). However, if the wind direction - and thus the wake - is not aligned with the line-of-sight from the lidar (panel b), then the same wake will be measured as generally wider, since the retrieval of the wake width is now affected by the relatively coarse radial resolution of the lidar coordinate grid. In the schematic diagram shown in Figure 10, at an arbitrary fixed downwind distance from the turbine, the (same) wake would be detected as 19% larger when it is not aligned with the line-of-sight from the scanning lidar. This result becomes more evident the when the laser beam is more perpendicular to the wake. This result is due to the aspect ratio of the lidar "pixels," and thus would affect other wake characterization approaches relying on instruments not co-located with the turbine such as in Banta et al. (2015); Aitken et al. (2014a), but would not affect nacelle-mounted wake measurements, such as in Bingöl et al. (2010); Aitken and Lundquist (2014) as nacelle-mounted wake measurements are usually aligned with the wake,

unless the wake is intentionally yawed (Fleming et al., 2016; Trujillo et al., 2016)."

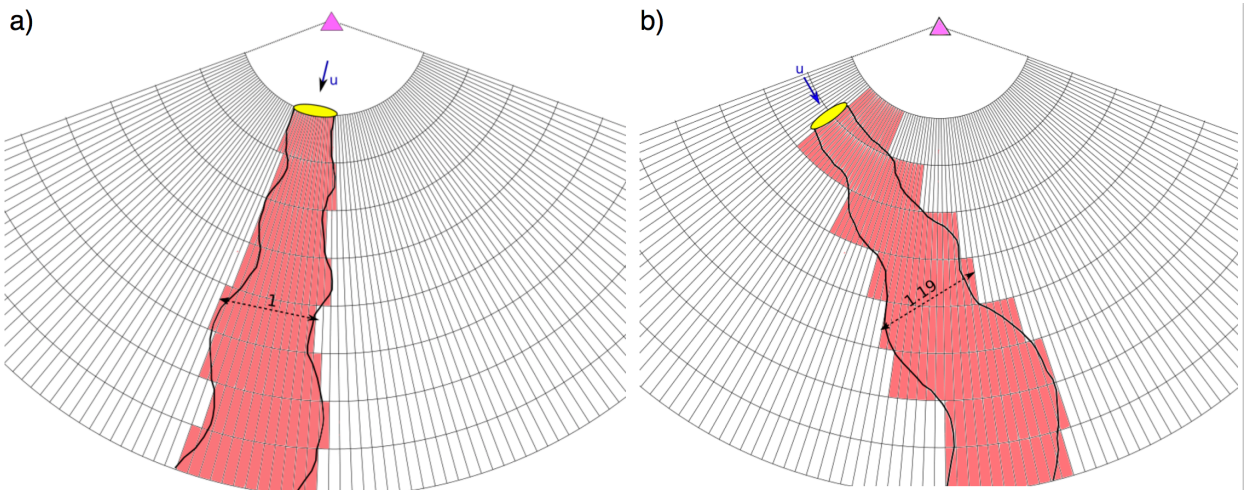

"Figure 10. Qualitative sketch of the dependence of detected wake width on the orientation of the coordinate grid used by a scanning lidar (purple triangle) as a function of the wind direction. Panel a shows the case of a wake aligned with the line-of-sight from the scanning lidar (wind direction shown by the blue arrow), while panel b shows the case of a wake not aligned with the line-of-sight from the lidar. The dashed arrow highlights the difference in the detected wake width for the two cases, at fixed downwind distance from the turbine (yellow ellipse)."

10. P12, Section 4.4: This comment relates to the Major Comments/Questions section above. Perhaps consider constructing a 3D volume of interpolated information, as opposed to compositing two horizontal planes for comparison. The change in wake centerline with height, supported by the presented measurements, is a really neat result of this study. The actual shape of the ellipsoid could potentially be better described (and compared to previous measurements) if the data were constructed in a 3D framework.

As already mentioned before, we thank the reviewer for their suggestion of a 3D volume of interpolated data; however, we decided not to implement this in our present work. At any rate, the results presented in Section 4.4 do NOT compare two horizontal planes, but two vertical regions, as shown in Figure 9 and in Figure 11, which we think is much more simple and intuitive than a real 3D framework to show our main finding of the vertical stretching of the structure of a wake, but with a lower magnitude than the ambient veer.

11. P12, L28: Why were the data separated between 55-75 m and >75 m, especially given hub height is at 80 m and data exist below 55 m within the rotor sweep. Why was the lower region bound vertically by 20 m but the upper region allowed to be larger? A quick comment on why this method was chosen could be beneficial.

The lower bin of data is between 35 and 55 m, and not between 55 and 75 as stated here. With this choice, we can have a great number of positions at low and high levels compared with the vertical dimensions of the turbines. By choosing these levels, we have an approximately equal number of vertical positions in each bin, given the geometry shown in Figure 2. To make this clear, we will include the following sentence: "these levels were chosen to create bins at low and high heights, compared to the vertical dimension of the turbines, with approximately the same number of vertical positions where the lidar measurements were taken, as shown in Figure 2".

MINOR EDITS:

1. P2, L16: "four" instead of 4.

2. P4, L15: The period at the start of this line should be at the end of the previous line.

3. P4, L23: "six" instead of 6.

4. P6, L14: Insert a period after (MAD).

5. P7, L11: Insert the word "the" between "as independent".

6. P9, L19: MAD is already defined on P6.

Thank you for catching all these edits! The manuscript will be changed accordingly.

2. Review #2

In this document, the reviewer comments are in black, the authors responses are in red.

The authors thank Dr. Nygaard for his detailed review and useful suggestions to improve the quality of our work.

Summary: this paper presents single lidar measurements of multiple wind turbine wakes. A wind field reconstruction model is used to derive wake characteristics from the line of sight wind speeds. The presented model is an extension to multiple wakes of a previous model developed by the same research group to characterize a single wake. Results are presented for the decay of the velocity deficit and the increase of the wake width with downstream distance. The wake centerline is found to shift orientation with height, indicating stretching of the wake profile in veered flow. The results are interesting and add to the developing picture of wakes in wind farms.

Thank you for finding our results interesting!

The method is sound, but could have been better explained, especially with regards to the vertical dimension and the influence of multiple elevation tilts (see specific comments below). The authors find some differences between the outer and the inner turbines in a row, but no explanation for these differences is offered.

The paper is definitely worthy of publication, but I suggest the authors consider the questions and suggestions below to improve the presentation of the methodology and the results.

Questions and suggestions:

In the model of Eq. (4) there is no reference to the vertical dimension or the elevation angle. Is it supposed to be applied at a fixed elevation angle? It is unclear how the vertical structure of the wakes is considered. At a fixed elevation angle the laser beam will probe at increasing height with increasing range. Were multiple elevation tilts combined in figures 7 and 8 to account for this?

Yes, equations (3) and (4) are applied at each fixed elevation angle. Then, to compute results in Figure 7 and 8, all the six elevation angles used in the campaign are combined to produce the final results.

To make this clear, we will modify the sentence that introduces our models as follows: “At a fixed elevation angle, the line-of-sight velocity u_LOS can be related to …”.

Moreover, to make clear that Figures 7 and 8 use data from all the elevation angles, we rephrased the sentences below as follows:

- "Figure 7 shows velocity deficit versus downwind distance from the turbines, calculated from the 276 PPI scans (at all the elevation angles) performed during the whole night (stable conditions) of 26 August 2013."
- [Caption of Figure 7] "Continuous lines represent the median values calculated from the PPI scans performed at all the considered elevation angles during the night (stable conditions) of 26 (panel a) and 23 (panel b) August 2013".
- [Caption of Figure 8] "Wake width vs downwind distance from the turbines, for the wakes of the four turbines in the studied row, from PPI scans performed at all the six considered elevation angles."

Consider adding a reference to Wang and Barthelmie - Journal of Physics: Conference Series 625 (2015) 012017 - Wind turbine wake detection with a single Doppler wind lidar. This has a similar wake wind field reconstruction method.

We will add a reference to this paper in the introduction.

P1, L23: The reduction in power for turbines in wake can exceed the 40% mentioned as the upper limit. As is well known, it is very sensitive to wind direction, being largest when the wind is aligned with rows of turbines. Also the observed maximum reduction depends on the size of the wind direction sector over which the data are averaged. But even for a 30 degree sector Nygaard 2014 found reductions of up to 60% for certain conditions. The total wake loss considering all wind directions and wind speeds is typically less than 20%. My point is that the 40% mentioned in the text is a meaningless number without further context. It only applies for certain wind directions and for averaging over a sector of a certain size. I invite you to make the context of this number clearer or to consider, if a specific value is needed.

Thank you for pointing out that we should have been more careful with this. Since, as you explained, giving a precise number for this energy reduction is not possible, we will eliminate this sentence from the manuscript, and include the references to Barthelmie et al. 2010 and Nygaard 2014 in the previous sentence, along with other papers which deal with energy reductions in wakes.

P2, L11: the appropriate reference for the Jensen model is N. O. Jensen, A note on wind generator interaction, Risø-M-2411 (1983). The reference you have to Jensen 1984 was new to me, so thank you for pointing it out. However, on a quick browse through that paper I did not see any mentioning of the Jensen wake model. The Jensen 1983 report is often cited together with the 1986 paper by Katic, Højstrup and Jensen, which introduces the method of wake superposition employed in the Park model in WAsP.

Thank you for the useful suggestion. We will modify the reference, which will include Jensen

1983 and Katic et al. 1986.

P2, L28: it is important to include more references on capturing multiple wakes in wind farms. At present only two are listed. But since this is the main focus of the paper it is crucial to establish the existing state of this area of study. “Among others” is insufficient. Here are some suggestions: Hirth et al., Wind Energy 18, 529 (2015) - Coupling Doppler radar-derived wind maps with operational turbine data to document wind farm complex flows, Hirth et al., Wind Energy (2015) - Dual-Doppler measurements of a wind ramp event at an Oklahoma wind plant, Kumer et al., Energy Procedia 80 245 (2015) - Characterisation of single wind turbine wakes with static and scanning WINTWEX-W LiDAR data (already cited elsewhere in the paper), Wang and Barthelmie paper mentioned above, Van Dooren et al., Remote Sens. 2016, 8, 809 - A Methodology for the Reconstruction of 2D Horizontal Wind Fields of Wind Turbine Wakes Based on Dual-Doppler Lidar Measurements

Thank you for pointing out that we should improve the references here. We will substantially improve this paragraph with the references you suggest: “The interactions between multiple wakes must be captured in studies of large wind farms, as done by Clive et al. (2011); Hirth et al. (2015a, b); Kumer et al. (2015); Wang and Barthelmie (2015); Aubrun et al. (2016); van Dooren et al. (2016).”.

P3, L12: a photo or photo collage would greatly assist the understanding of the setup of the field campaign, the description of the surroundings and possibly the interpretation of the results.

The following pictures showing the instruments at the site of the campaign (and its land use) will be included in the Supplementary Material.

Figure 1: scanning lidar co-located with WC-3, looking to the southwest (photo courtesy Paul Quelet)

Figure 2: WC-1, looking towards SE (photo courtesy Lundquist)

Figure 3: WC-3 looking to SE (photo courtesy Lundquist)

Figure 4: WC-2 looking to SE (photo courtesy Paul Quelet)

P3, Fig.1: the figure is good, but should only include the relevant information. Were all the surface flux stations used in determining the atmospheric stability? Were all profiling lidars used in the analysis? Leave out the details not connected with this paper.

Although we agree that the figure includes some instruments that were not directly used in our work, we still think that it is important to give a complete overview of the set-up of the instruments at the campaign. However, we will improve our description in the manuscript to make clear which instruments we used for our research.

Regarding the different surface flux stations, we will include the following sentence in Section 2.1.2 to clearly states which station we used in our work: "We used measurements from the surface flux station ISU_3 to assess atmospheric stability conditions, with the calculation of Obukhov length".

Regarding the different vertical profiling lidars, see the comment below.

Sec 2.1: the text should specify clearly how the profiling lidars were used in the analysis. Section 2.1 has a brief mention of a comparison between the scanning lidar and WC-3. How was this done? What did the results show? WC-3 was used to determine veer on page 14, but please introduce this in the description of the observational dataset. Was WC-2 used for anything in the present study?

Thank you for noticing that we should be more clear regarding how we used data from the different instruments deployed at the site. Regarding the comparison between WC-3 data and scanning lidar data, the manuscript already includes the reference to the Vanderwende's et al. paper where this comparison is described in detail. Our paragraph includes the following sentence about the results: "Vanderwende et al. (2015) demonstrated good agreement between the co-located scanning and WC-3 profiling lidar measurements at the altitudes where measurements overlapped."

Regarding how we used data from the different profiling lidar, we will add this sentence in the description of the observational dataset: "At CWEX-13, southerly wind conditions dominated the campaign. So, we used data from the WC-1 profiling lidar to measure upwind conditions for the studied row of turbines, and calculate the ambient wind veer." We did not use data from WC-2 and WC-3 in the retrievals of wake characteristics.

P4, L15: the period at the beginning of the line belongs at the end of the previous line Sec.2.1.1: I miss a detailed description of the scan patterns. What was the sector size for the PPI scans? What was the time per scan? This is hinted at on P14, but it belongs in this section. What was the order of the RHI and PPI scans? Am I right that the RHI scans are not used in the present analysis? If that is correct, then please state that. Was the pointing accuracy of the scanning lidar checked using hard target returns (eg from the wind turbines)? This information is important to interpret the results and should be included. Alternatively, if the authors have made this information available elsewhere, a reference could suffice.

Thank you for pointing out that we did not provide this piece of information in the proper location and that we should provide a more detailed description of the scan patterns. We will add the following sentence: "each PPI scan lasted approximately 100 seconds, spanning an azimuth range of 50deg with a speed of 0.5deg/s, while a RHI had a duration of about 30 seconds." We will also add the following table with more details about the scans performed during the field campaign:

Table 2. *Description of the 30-min cycle of scanning lidar scans in CWEX-13 field campaign. The characteristic fixed angle refers to the elevation angle for PPI and VAD scans, the azimuth angle for RHI scans.*

number of scans	type of scan	characteristic fixed angle	duration of each scan	cumulative time
2	VAD	75°, 60°	132 s	0:00 - 4:24
6	PPI	2.8°, 2.5°, 2.2°, 2.1°, 1.8°, 1.5°	104 s	4:24 - 14:48
3	RHI	160°, 170°, 180°	32 s	14:48 - 16:24
6	PPI	2.8°, 2.5°, 2.2°, 2.1°, 1.8°, 1.5°	104 s	16:24 - 26:48
6	RHI	160°, 170°, 180°, 180°, 170°, 160°	32 s	26:48 - 30:00

We did only use PPI scans to detect wakes, and this is stated at the beginning of section 3: "The line-of-sight velocity measured by the WINCDUBE 200S scanning lidar (Figure 3) during the horizontal (PPI) scans can be analyzed to determine wake characteristics and how they evolve in space as the wakes propagate."

P5, Fig. 2: how large was the change in elevation between the lidar location and the turbines? State what is was, then argue why it can be neglected. Otherwise, make an assessment of the uncertainty or bias it introduces into the results.

The change in elevation between the turbines and the scanning lidar was 7m. This will be included in the caption of the figure. However, we DID take into account this difference, as already stated in the caption itself.

P6, L3: the Monin-Obukhov length has dimensions of Length. I assume the listed limits should be in meter.

Thank you for noticing this. We will correct the manuscript accordingly.

P6, L6: insert a "The" at the beginning of the line. Same on line 23 after Figure 3.

We will add "the" in both the proposed sentences.

P6, L12: define carrier-to-noise ratio. Explain the filter on CNR (<-27dB) and why this is necessary. Why was this threshold chosen? How sensitive are the results to this value?

We will add more details regarding the CNR threshold: "First, a threshold is imposed to the carrier-to-noise ratio (CNR), which represents the strength of the backscattered signal compared to background noise (values closer to 0 dB indicate a stronger signal relative to the noise): all measurements with carrier-to-noise ratio CNR < -27 dB are discarded from further analysis [Vanderwende et al. 2015]. Measurements with a lower CNR often had unrealistically high (> 15

m/s) values of radial velocity; and this threshold value is comparable with choices in other studies [Cariou et al. 2011, Bastine et al. 2015, Debnath et al. 2016]."

P6, L13: do data refer to the line of sight wind speeds?

Yes. To make this clear, we will change the sentence in "…line-of-sight velocity data…".

P6, L13: define \mu and define MAD in an equation. Is the standard deviation equal to MAD (it is cryptically stated to be evaluated according to MAD)? How sure are you that the outliers removed are not physical? Do you know the source of the outliers you exclude?

We will improve the description of the MAD method as follows: "in each scan, line-of-sight velocity data which are not included in the interval $(\mu - 3\hat{\sigma}, \mu + 3\hat{\sigma})$, where μ is the average of the data, are removed from the analysis. The standard deviation $\hat{\sigma}$ is evaluated according to the median absolute deviation (MAD), assuming normally distributed data: $\hat{\sigma} = 1.4826\ \mathrm{MAD}$, where $\mathrm{MAD} = \mathrm{median}(|u_{LOS,i} - \mathrm{median}(u_{LOS})|)$".

The threshold was chosen as in Aitken et al. 2014, and, under the assumption of normally distributed data, 99.7% of data are included in the selected interval. Thus, the discarded values can be considered to be due to extreme events such as hard strikes.

P6, L23: I suggest inserting "the assumed" in front of uniform ambient wind speed.

Thank you for the suggestion. We will add "the assumed" in the sentence.

P7, L1: there is a "the" missing in front of ambient flow speed.

We will add "the" in the sentence.

P7: it would be very useful to have an overview image or map showing the turbine locations and the scanned sector.

The following figure, showing the location of the scanning lidar, of the four turbines, and the line-of-sight velocity measurements during two PPI scans (one for each of the studied days), will be added to the manuscript at the end of the "Lidar measurements" section. The Figure will be introduced in the paragraph as follows: "Figure 3 shows examples of maps of line-of-sight velocity measured by the scanning lidar during two PPI scans performed at night on the selected days. The wind turbine wakes can clearly be detected in terms of reduced wind speed downwind of the four wind turbines."

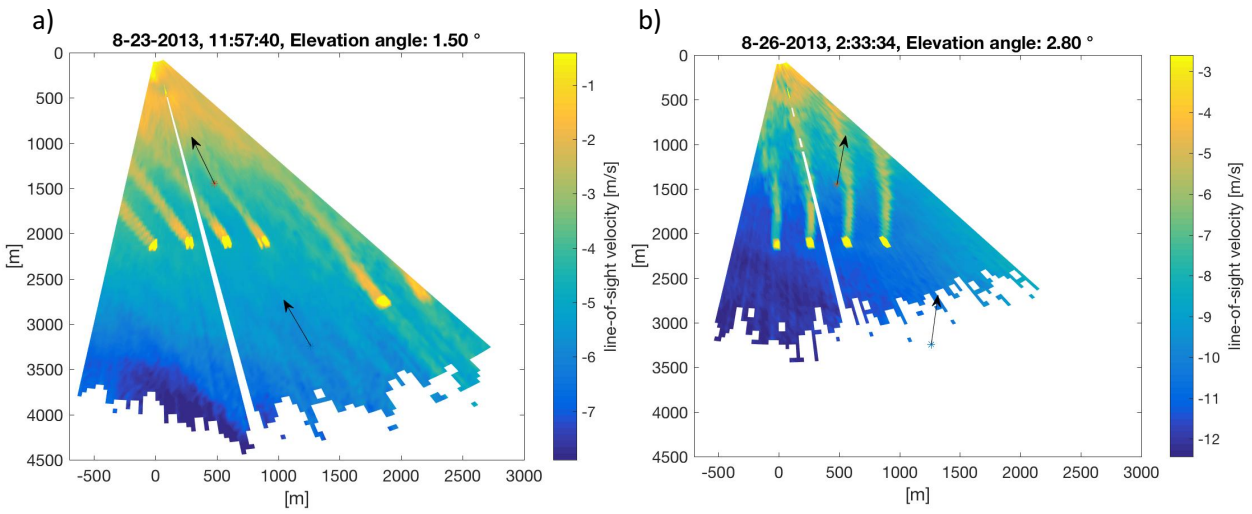

The caption of the Figure will be: "Figure 3. Color maps of line-of-sight velocity measured by the scanning lidar during two PPI scans performed at 11:57 UTC (6:57 am LDT) on 23 August 2013 (panel a) and at 02:33 UTC (9:33 pm LDT) on 26 August 2013 (panel b). The scanning lidar is located in the origin of the coordinate system. The two arrows show wind direction as measured by the profiling lidars WC-1 and WC-2 at 80 m AGL."

P7, Fig.3: to define the wind direction there should be an indication of the north (or south) direction in the figure. Is south upwards in the figure?

North is upwards in the Figure. To make this clear, we will modify the Figure adding a North direction arrow, and rephrase a sentence as follows: "…both alpha and phi are >0 for clockwise rotations from North."

P9, L19: MAD acronym was already defined. When the method was applied again, did you use the same bounds as on page 6?

We will eliminate "median absolute deviation" from the sentence since we already defined MAD previously. Yes, we used again 3 standard deviations as threshold. The sentence will be rephrased as: "the MAD method is applied again to discard wake characteristics which do not lie within three standard deviations of the mean".

P9, L20: "mean characteristic" – is this for the entire database or for a single scan?

Thank you for noticing that we didn't specify this clearly. The sentence will be rephrased as: "the mean characteristic at each range gate for each whole night".

P9 L21: define the Pearson correlation coefficient and the mean squared error.

We will rephrase the sentence as follows:

with Pearson correlation coefficient ($corr(u_{LOS}, \hat{u}_{LOS}; g) = cov(u_{LOS}, \hat{u}_{LOS}; g)/\sqrt{cov(u_{LOS}, u_{LOS}; g)cov(\hat{u}_{LOS}, \hat{u}_{LOS}; g)}$, where g represents the data weights) larger than 0.9 and mean squared error ($MSE = \frac{1}{\sum_{i=1}^{n} g_i} \sum_{i=1}^{n} g_i(\hat{u}_{LOS,i} - u_{LOS,i})^2$) lower than 0.5 are included in the final analysis of the results.

P10, Fig. 5: what do the corresponding plots of data availability look like? These could be important to include to understand if the some of the decrease in Figure 5 is driven by the measurements and not by wake characteristics. I would also like to know the number of scans included in the stable and unstable curve. Were there no neutral conditions?

Since we considered southwesterly (26 August 2013) and southeasterly (23 August 2013) flows, as the wakes go further from the turbines, they actually get closer to the scanning lidar (see scheme in Figure 1), so we are not concerned about data availability at long downwind distances (i.e. close to the lidar). However, the following plot showing data (line-of-sight velocity) availability for 23 and 26 August will be included in the Supplementary Material. The vertical dashed lines show the positions of the turbines. As can be seen, the data availability for all the range gates considered in Figure 5 (i.e. to the left of the dashed lines) is nearly 100%, and so our results are not affected by this possible issue.

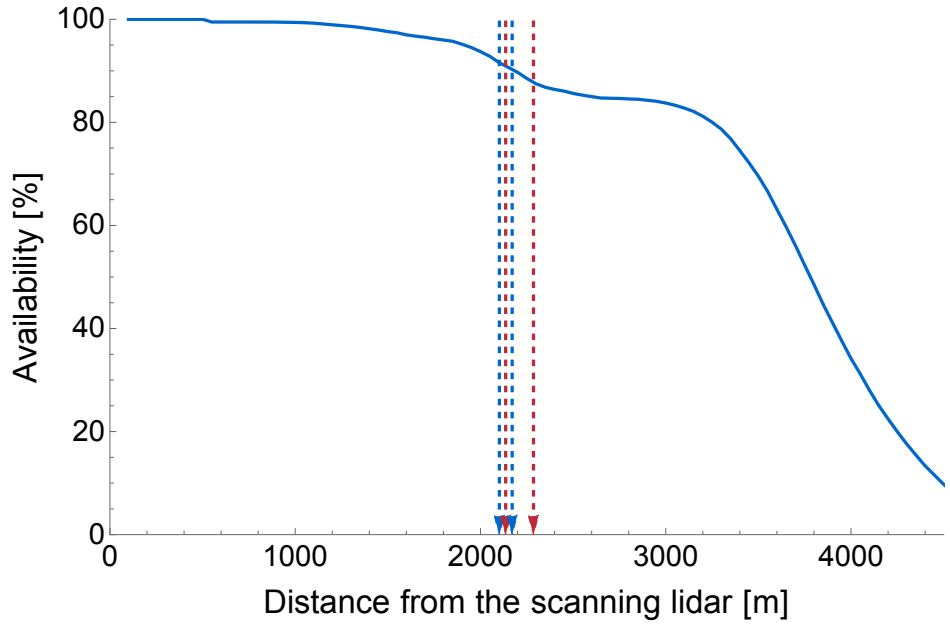

Regarding neutral conditions, we will add the following sentence to the caption of the Figure: "(neutral conditions were detected only for very short periods, and are not included here)". So, nearly all the PPI scans performed during the selected days are included in Fig. 5.

P11, Fig. 6: are these plots along the wake centerlines? What was the wind direction and how was

it oriented with respect to the turbine row? This can be deduced from figures 8 and 9, but you might as well make it clear here.

Considering how we modeled each wake (equation 4) and how we defined the velocity deficit (equation 5) in the wake, the velocity deficit is by definition calculated at the location of the center of the wake – thus the wake centerline. Regarding the wind direction, it is stated in Section 2.1.1 that 26 August shows predominant southwesterly wind. However, as a reminder, the caption of the figure will include: "… 26 August 2013, southwesterly wind, …".

P11, Fig. 7: the authors should attempt to explain the differences they see. While the two outer turbines both have smaller deficits than the inner turbines, the difference in deficit between the two outer turbines is larger than the difference between the inner turbine and the outer turbine with the highest deficit. It would be useful to label the curves with the turbines they belong to. Could there be a relation with the vertical structure of the wakes and sampling the wakes at different heights. As stated above it is important to know how the different elevation tilts were combined (or not) in making this figure. Is the width of the shaded bands one or two standard deviations? I suggest making the same plot for the 23 August data.

We will change the Figure as follows to highlight the behavior of the single turbines:

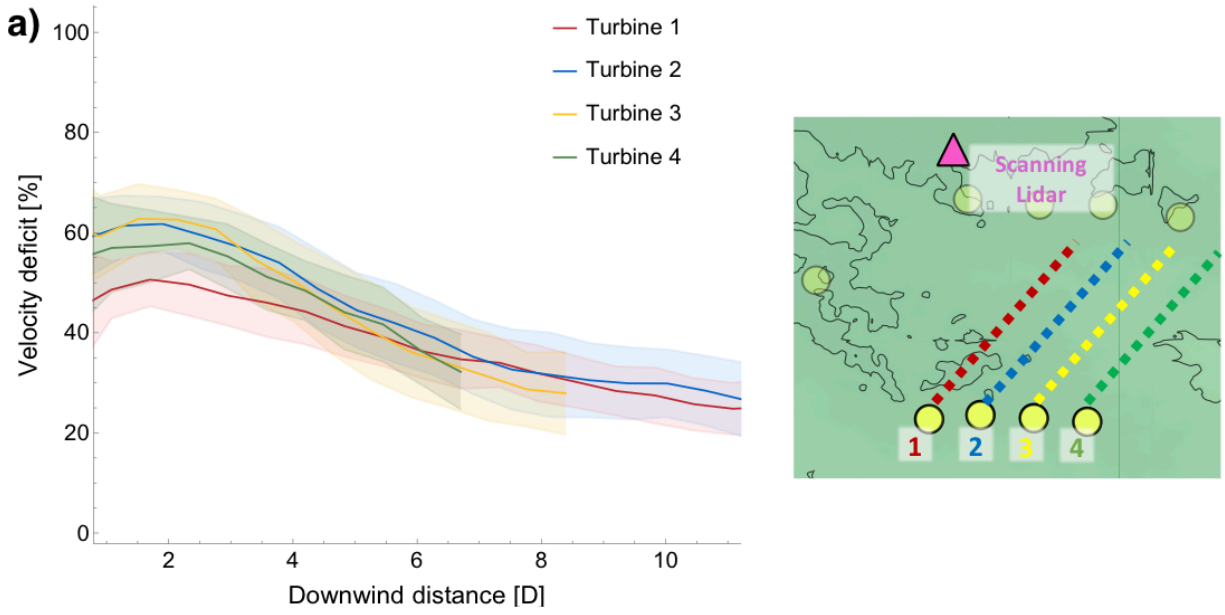

And we will include the following plot from 23 August:

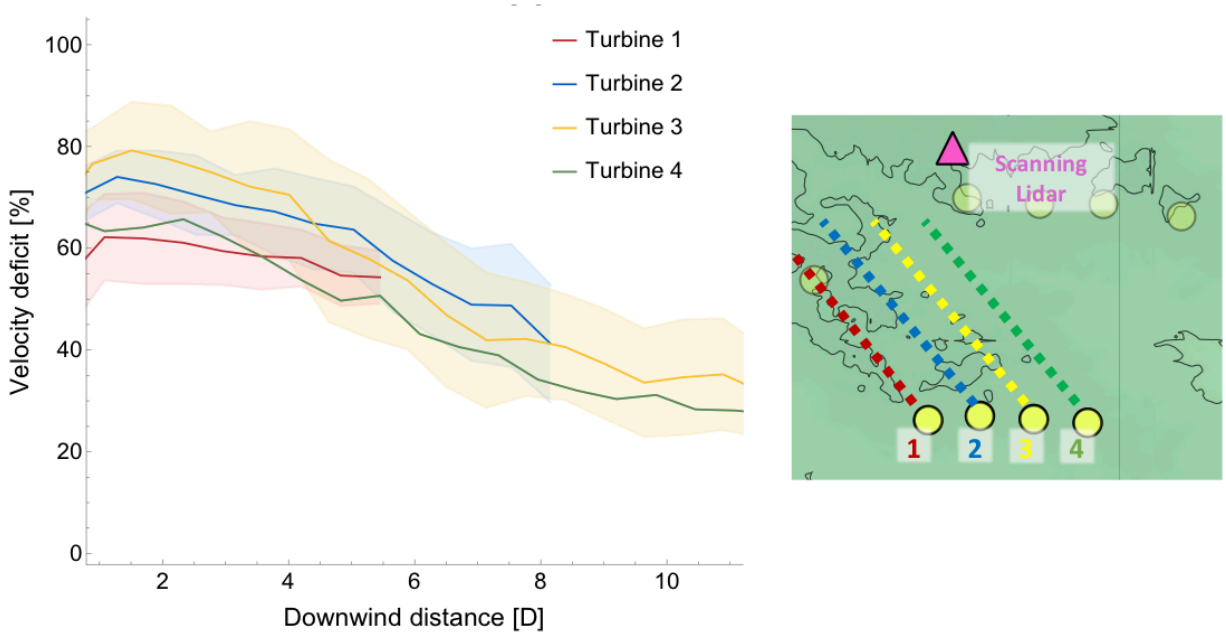

The paragraph which introduces this new version of the Figure will be changed accordingly: "Figure 7 shows velocity deficit versus downwind distance from the turbines, calculated from the 276 (242) PPI scans, at all the elevation angles, performed during the whole night - stable conditions - of 26 (23) August 2013."

As can be seen, for the 23 August 2013 the difference between outer (turbines 1 and 4) and inner (turbines 2 and 3) wakes is more consistent for all the studied turbines, and the phenomenon noticed by the reviewer does not appear. Therefore, we cannot infer general results beyond what we stated in the paragraph: "wakes from outer turbines (number 1 and number 4), have lower velocity deficits than the wakes from inner turbines (number 2 and number 3), for relatively small downwind distances, with a difference up to 15%".

Regarding the use of different elevation angles, the caption of the Figure will include: "Velocity deficit vs downwind distance, for the four wakes of the studied row of turbines. Continuous lines represent the median values calculated from the PPI scans performed at all the considered elevation angles during the night (stable conditions) of 26 (panel a) and 23 (panel b) August 2013;".

Regarding the shaded bands, we will rephrase the description in the caption as "shaded areas show ± one standard deviation of the data" (and the same was added for the caption of Figure 8).

P 11, L 4: replace low with small

We will replace the adjective. Thank you for suggesting!

P12, L 12: the passive voice makes it hard to understand the sentence. Consider rephrasing it. I think you mean widest, when you write largest.

We are not sure which passive voice you refer to. In any case, we will slightly rephrase the sentence as: "…the scanning lidar systematically identifies as the widest the wake which, at a given downwind distance, is the most perpendicular to the laser beam…".

P16, Fig. 11: I am not sure I agree with the conclusion of a larger angular difference for the outer turbines based on the linear fits. The linear fits are very poor. Indeed, the data could be seen as describing an oscillation, where the inner and outer turbines follow each other.

We agree that the quality of the linear fits is rather poor, however we think they are useful to show the different behavior between wakes from inner and outer turbines. To make this clear and to include your suggestion about oscillations, we will rephrase the description of these results as follows: "as suggested by the linear regression fits, wakes from outer turbines often present a larger angular difference in wake centerlines compared to wakes from inner turbines, though with variability for different veer values that motivates further study".

P20, L16: &amp should be &.

Thank you for catching this mistake!

P21, L14: Spera, D should be Neustadter, H. E. and Spera, D. and the page number is 240 not 241.

Thank you for noticing. We will correct the reference accordingly.

3. Review #3

In this document, the reviewer comments are in black, the authors responses are in red.

The manuscript entitled "Three-dimensional structure of wind turbine wakes as measured by scanning lidar" deals with the analysis of field measurements performed during stable atmospheric conditions on the velocity field downstream of a group of four wind turbines, captured by a scanning LiDAR.

The study is of great interest for the wind energy community since it can contribute to better quantify the wind turbine wake properties and so, to validate some wake models and numerical simulations.

The authors thank the reviewer for their time in reviewing this contribution and we are pleased that this work is considered of great interest.

The experimental set-up is well detailed, the method to detect the wake locations of multiple wakes on each snapshot is well described and the content is well structured. On the other hand, the discussion is rather poor: several results, which are not intuitively expected, are mentioned but not justified. For instance:

Thank you for pointing out that the discussion of the results should be improved. We will justify our results as explained in the next paragraphs.

- The reason why the velocity deficit is smaller for outer wakes than for inner wakes. Is it possible to give an explanation without having information about the wind turbine operating conditions? The velocity deficit is also primarily related to the power coefficient of the wind turbine.

To provide a possible explanation of this result, we will include the following sentence at the end of Section 4.2: "The presence of outer turbines seems to reduce the effectiveness of lateral entrainment of faster air to recover wind conditions in the inner wake regions of the wind farm." Moreover, to provide additional insight, the plot with the results for the 23 August will be included in the revised manuscript.

The turbines are all the same model of turbine and therefore would have the same power coefficient at each wind speed regime, and we have verified (not shown as the data are not publicly available) that the turbines are all producing, on a daily average basis, within 15kW and 31kW of each other during 23 and 26 August 2013, respectively.

- The reason why the wake width is dependent on the relative position between the wake and the

scanning lidar. Please elaborate an explanation.

Thank you for pointing out that we did not provide a sufficient discussion for this. We will add the following paragraph and Figure to our manuscript:

"This result is due to the relationship between the viewing angle and the aspect ratio of the lidar retrieval "pixels", which are related to the relatively long range gate (50 m) and relatively narrow azimuthal resolution (0.5 degree). As qualitatively shown in the schematic of Figure 10, the scanning lidar measures the line-of-sight velocity in narrow pencil-shaped "pixels". With this geometry, if the wind direction - and thus the wake - is aligned with the line-of-sight from the lidar, the wake width can be assessed with high precision due to the high azimuthal resolution in each pencil-shaped area (panel a). However, if the wind direction - and thus the wake - is not aligned with the line-of-sight from the lidar (panel b), then the same wake will be measured as generally wider, since the retrieval of the wake width is now affected by the relatively coarse radial resolution of the lidar coordinate grid. In the schematic diagram shown in Figure 10, at an arbitrary fixed downwind distance from the turbine, the (same) wake would be detected as 19% larger when it is not aligned with the line-of-sight from the scanning lidar. This result becomes more evident the when the laser beam is more perpendicular to the wake. This result is due to the aspect ratio of the lidar "pixels," and thus would affect other wake characterization approaches relying on instruments not co-located with the turbine such as in Banta et al. (2015); Aitken et al. (2014a), but would not affect nacelle-mounted wake measurements, such as in Bingöl et al. (2010); Aitken and Lundquist (2014) as nacelle-mounted wake measurements are usually aligned with the wake, unless the wake is intentionally yawed (Fleming et al., 2016; Trujillo et al., 2016)."

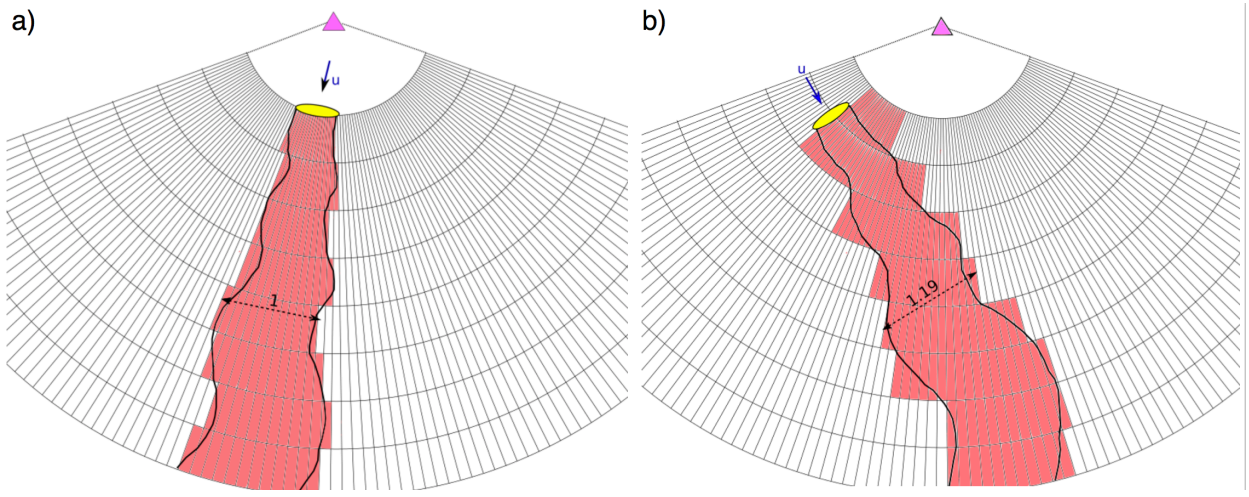

"Figure 10. Qualitative sketch of the dependence of detected wake width on the orientation of the coordinate grid used by a scanning lidar (purple triangle) as a function of the wind direction. Panel (a) shows the case of a wake aligned with the line-of-sight from the scanning lidar (wind direction

shown by the blue arrow), while panel (b) shows the case of a wake not aligned with the line-of-sight from the lidar. The dashed arrow highlights the difference in the detected wake width for the two cases, at fixed downwind distance from the turbine (yellow ellipse)."

- The correlation between the veer and the wake stretching angle is rather poor (figure 11), the data present a very high scatter, with no linear trend. It is hazardous to make some interpretation with this plot. Parallel to the previous remark on the dependence of wake widths to lidar beam orientation, could the measurement set-up and the scanning lidar limitations be responsible of this wake stretching, instead of the veer? Again, the conclusion that the inner and outer wakes behave differently with the veer effect must be justified.

We agree that the quality of the linear fits is rather poor, however we think they are useful to show the different behavior between wakes from inner and outer turbines. To make this clear and to include the suggestion of another reviewer about oscillations in this relationship, we will rephrase the description of these results as follows: "as suggested by the linear regression fits, wakes from outer turbines often present a larger angular difference in wake centerlines compared to wakes from inner turbines, though with variability for different veer values that motivates further study".

We do not think that the measurement set-up may have affected this result, since the same results are obtained for both 23 and 26 August (i.e. for different wind directions), while for the wake width different wind directions caused different results.

To provide a possible explanation for this result, we will add the following paragraph at the end of Section 4.4.1: "A possible physical explanation for this phenomenon can be detected in the interaction between wake rotation due to rotating blades and wind veer. The blades of the wind turbines in CWEX-13 wind farm rotate clockwise and so the downwind wakes rotates counter-clockwise [Burton 2001]. The wake can thus be considered as a sort of plume with its own momentum and rotation, which interacts with the ambient veer, that in turns tends to rotate the wake in the opposite direction (in the Northern hemisphere), thus causing a reduction in the global wake vertical stretching than would be present if only the ambient veer affected the wake. Inner wakes seem to be less subject to the effect of ambient wind veer, as if the presence of outer turbines reduces the ability of ambient wind characteristics to reach and impact inner regions of the wind farms."

Minor comments:

- Page 4, line 12: 30-min cycle: do you mean that, during 30 minutes, several PPI and RHI are collected? If yes, please indicate the duration to collect one PPI and one RHI. It will give an idea of the temporal resolution of the obtained velocity field.

Yes, several PPI and RHI scans are collected in each 30-min cycle. To make this clear, the revised text will include the following sentence: “each PPI scan lasted approximately 100 seconds, spanning an azimuth range of 50deg with a speed of 0.5deg/s, while a RHI had a duration of about 30 seconds”. A table will also be included (see comment below) with more details about the 30-min cycle.

- Give the range of azimuth angles that have been scanned during PPI and RHI. A table with all these information would be appropriate.

The following table with a detailed description of the scans performed during the experiment will be included in the manuscript:

Table 2. *Description of the 30-min cycle of scanning lidar scans in CWEX-13 field campaign. The characteristic fixed angle refers to the elevation angle for PPI and VAD scans, the azimuth angle for RHI scans.*

number of scans	type of scan	characteristic fixed angle	duration of each scan	cumulative time
2	VAD	75°, 60°	132 s	0:00 - 4:24
6	PPI	2.8°, 2.5°, 2.2°, 2.1°, 1.8°, 1.5°	104 s	4:24 - 14:48
3	RHI	160°, 170°, 180°	32 s	14:48 - 16:24
6	PPI	2.8°, 2.5°, 2.2°, 2.1°, 1.8°, 1.5°	104 s	16:24 - 26:48
6	RHI	160°, 170°, 180°, 180°, 170°, 160°	32 s	26:48 - 30:00

- Page 5, figure 5: the y-axis legend indicates “detected wakes [% scans]” but the maximum value is 1, and not 100.

Thanks for noticing this incongruity. We will revise the plot accordingly.

Three-Dimensional Structure of Wind Turbine Wakes as Measured by Scanning Lidar

Nicola Bodini[1,2], Dino Zardi[2], and Julie K. Lundquist[1,3]

[1]Department of Atmospheric and Oceanic Sciences, University of Colorado Boulder, Boulder, Colorado, USA
[2]Department of Civil, Environmental and Mechanical Engineering, University of Trento, Trento, Italy
[3]National Renewable Energy Laboratory, Golden, Colorado, USA

Correspondence to: Nicola Bodini (nicola.bodini@colorado.edu)

Abstract. The ~~slower~~ lower wind speeds and increased turbulence that are characteristic of turbine wakes have considerable consequences on large wind farms: turbines located downwind generate less power and experience increased turbulent loads. The structures of wakes and their downwind impacts are sensitive to wind speed and atmospheric variability. Wake characterization can provide important insights for turbine layout optimization in view of decreasing the cost of wind energy. The CWEX-13 field campaign, which took place between June and September 2013 in a wind farm in Iowa, was designed to explore the interaction of multiple wakes in a range of atmospheric stability conditions. Based on lidar wind measurements, we extend, present, and apply a quantitative algorithm to assess wake parameters such as the velocity deficits, the size of the wake boundaries, and the location of the wake centerlines. We focus on wakes from a row of four turbines at the leading edge of the wind farm to explore variations between wakes from the edge of the row (outer wakes) and those from turbines in the center of the row (inner wakes). Using multiple horizontal scans at different elevations, a three-dimensional structure of wakes from the row of turbines can be created. Wakes erode very quickly during unstable conditions, and can in fact be detected primarily in stable conditions in the conditions measured here. During stable conditions, important differences emerge between the wakes of inner turbines and the wakes of outer turbines. Further, the strong wind veer associated with stable conditions results in a stretching of the wake structures, and this stretching manifests differently for inner and outer wakes. These insights can be incorporated into low-order wake models for wind farm layout optimization or for wind power forecasting.

1 Introduction

A wind turbine wake is the volume downwind of a wind turbine, affected by the fact that the wind turbine removes momentum from the flow, thus reducing the downwind speed. ~~In this~~ Also, in the wake, the flow is more turbulent than in the inflow, because of the rotation of turbine blades and the presence of the wind turbine itself as an obstacle to the incoming wind flow (Landberg, 2015).

Wind turbine wakes impact the layout optimization and energy production of large wind farms (Brower, 2012). In fact, the reduced wind speed in the wake region has a direct effect on the ~~generation of power~~ power extracted by downwind turbines ~~(Neustadter and Spera, 1985; Nygaard, 2014). Barthelmie et al. (2010) found up to a 40% reduction in the power generated by~~

~~turbines in wakes as compared to leading-edge or unwaked turbines.~~ (Neustadter and Spera, 1985; Barthelmie et al., 2010; Nygaard, 2014). Moreover, the increased turbulence in wakes enhances turbulent loads for downwind turbines, possibly inducing premature failure (Crespo et al., 1999; Sathe et al., 2013).

Therefore, wakes need to be studied and understood in order to maximize the efficiency of wind energy production. In particular, wake models are applied in several steps of the design and life-time management of wind farms~~: layout of wind farms~~ , whose layout is studied in detail ~~, in order~~ to maximize the amount of energy generated by the turbines (Elkinton et al., 2006; Samorani, 2013). Moreover, the overall wind resource assessment process needs to take into account the effect of wakes to have a reliable prediction of future power production (Brower, 2012; Clifton et al., 2016). Lastly, wind farm control techniques incorporate detailed studies of wake characteristics while periodically changing some features of the turbines (such as yaw angle and pitch angle) in order to maximize the overall power production from the whole wind farm (Fleming et al., 2014, 2016; Gebraad et al., 2016; Vollmer et al., 2016b). Typically, all these processes are computationally intensive, and apply low-order models of turbine wakes (Elkinton et al., 2006; Chowdhury et al., 2012), such as the Jensen model ~~(Jensen et al., 1984)~~(Jensen, 1983; Katic et al., 1986). In this way, several scenarios can be tested, but these lower-cost models oversimplify reality and may not be capable to fully represent wake characteristics in a detailed and realistic way (Barthelmie et al., 2006; Andersen et al., 2014).

Atmospheric stability has been shown to have a major impact on wind turbine wake evolution and wind farm performance in both observational (Magnusson and Smedman, 1994; Hansen et al., 2012; Wharton and Lundquist, 2012; Vanderwende and Lundquist, 2012; Barthelmie et al., 2013; Dörenkämper et al., 2015; Machefaux et al., 2015; Mirocha et al., 2015) and modeling studies (Churchfield et al., 2012; Aitken et al., 2014b; Mirocha et al., 2014; Machefaux et al., 2015; Abkar and Porté-Agel, 2015; Abkar et al., 2015): wakes in stable conditions persist for long distances downwind, while during unstable conditions the enhanced turbulent mixing erodes the wakes more quickly.

Wake characterization from field data can validate and improve the quality of numerical models. Data from field campaigns avoid possible limitations of wind tunnel simulations, such as down-scaled geometric dimensions and low Reynolds number (Iungo et al., 2013). Lidars and radars have been widely used recently to characterize wind turbine wakes. These instruments can measure wind characteristics above the heights of most traditional meteorological towers, and they can be deployed and moved rather easily, allowing measurements at several different locations. Many wake validation studies from remote sensing measurements focus on individual isolated turbines (Käsler et al., 2010; Bingöl et al., 2010; Trujillo et al., 2011; Hirth et al., 2012; Hirth and Schroeder, 2013; Aitken et al., 2014a; Aitken and Lundquist, 2014; Bastine et al., 2015; Kumer et al., 2015), with some studies that aim at reconstructing the 3-dimensional structure of wind turbine wakes (Iungo et al., 2013; Banta et al., 2015). The interactions between multiple wakes must be captured in studies of large wind farms~~: see Clive et al. (2011); Aubrun et al. (2016) among others~~, as done by Clive et al. (2011); Hirth et al. (2015a, b); Kumer et al. (2015); Wang an

In this paper, we analyze scanning lidar and profiling lidar measurements from the CWEX-13 field campaign in a large wind farm in Iowa, and we extend the individual wake detection algorithm proposed by Aitken et al. (2014a) to characterize multiple wakes. The three-dimensional structure of wakes from a row of four turbines is assessed, in terms of velocity deficit, width of the wakes, and wake centerlines. Section 2 describes the CWEX-13 field campaign and how we use measurements from the

Table 1. Technical specifications of the studied wind turbines in CWEX-13 field campaign.

Rotor diameter (D)	80 m
Hub height	80 m
Rated power	1.5 MW
Cut-in wind speed	3.5 m s^{-1}
Rated power at	11 m s^{-1}
Cut-out wind speed	20 m s^{-1}

instruments deployed at the site. In Section 3 we present the wake characterization algorithm for multiple wakes, an expansion of the algorithm proposed by Aitken et al. (2014a). Section 4 highlights how wake characteristics (velocity deficit, wake width, and wake centerline) change in three-dimensional space, and for the first time we quantify the effect of ambient wind veer on the vertical stretching of the structure of wakes. In Section 5 we compare the present results with those obtained in previous studies, and we suggest possible future work to improve wake simulations and models.

2 Data and Methods

This study analyzes the scanning lidar and profiling lidar measurements from the CWEX-13 observational campaign, summarized in Takle et al. (2014) and Vanderwende et al. (2015).

2.1 CWEX-13 Observational dataset

CWEX-13 campaign (Lundquist et al., 2014) took place between late June and early September 2013 in a wind farm in central Iowa, the same wind farm studied in previous CWEX campaigns; however, CWEX-13 focused on a part of the wind farm that is different from what is discussed in Rajewski et al. (2013), Rhodes and Lundquist (2013), Mirocha et al. (2015), and Lee and Lundquist (2017). The region exhibits strong diurnal cycles of atmospheric stability, and frequent nocturnal low-level jets (Vanderwende et al., 2015). The area has a flat topography, with large fields of corn (height $1-2$ m) and soybeans (height $0.3-0.8$ m). The region also has four small villages, some riparian regions, and a few trees and buildings.

Figure 1 shows a schematic diagram of the area of the wind farm of interest in CWEX-13. The yellow dots represent the wind turbines, whose main technical specifications are reported in Table 1. For the purpose of this work, we focus on the characterization, using scanning lidar data, of the wakes from the row of ~~4~~ four turbines enclosed in the purple ellipse in Figure 1.

2.1.1 Lidar measurements

~~As shown by the scheme in Figure 1, three vertical profiling lidars and a scanning lidar were deployed at the site during the field campaign.~~ Three WINDCUBE v1 vertical profiling lidars (blue diamonds in Figure 1) were deployed at the site during the

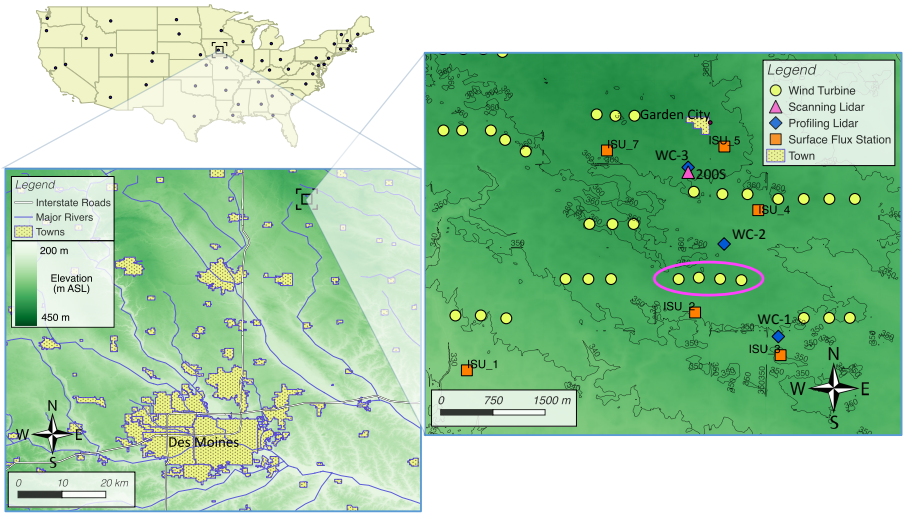

Figure 1. Schematic view of the part of the wind farm in central Iowa where the CWEX-13 field campaign took place. The row of ~~4~~ four turbines whose wakes are detected by the scanning lidar is highlighted in a purple ellipse.

field campaign, and they were located south of the studied row of four turbines, $8.5D$ north of the above-mentioned turbines, and $5.7D$ north of a second row of turbines. These instruments provided vertical profiles of wind speed and direction from 40 m to 220 m above the surface, with measurements collected every 20 m. At CWEX-13, southerly wind conditions dominated the campaign. So, we used data from the WC-1 profiling lidar to measure upwind conditions for the studied row of turbines, and calculate the ambient wind veer.

From 31 July to 6 September 2013, a LEOSPHERE WINDCUBE 200S scanning lidar was deployed with the northernmost WINDCUBE v1 profiling lidar (WC-3 in Figure 1). Vanderwende et al. (2015) demonstrated good agreement between the co-located scanning and WC-3 profiling lidars measurements at the altitudes where measurements overlapped. Scanning lidars can operate sweeping the azimuth angle with a constant elevation angle, the so-called *plan-position-indicator* (PPI) mode (*velocity azimuth display* - VAD - mode when a full conical scan is conducted), or sweeping the elevation angle while holding the azimuth angle fixed, in the so-called *range-height-indicator* (RHI), mode (Sathe and Mann, 2013). In CWEX-13, the scanning lidar used a combination of ~~both PPI~~PPI, VAD and RHI scans, with a 30-minute cycle ~~.~~ (each PPI scan lasted approximately 100 seconds, spanning an azimuth range of 50° with a speed of $0.5°s^{-1}$, while a RHI had a duration of about 30 seconds, see Table 2). Measurements were collected with slant range gates of 50 m at ranges up to 5000 m from the instrument, with an angular resolution of ~~0.1°~~0.5°. Line-of-sight (radial) velocity was measured with an accuracy better than 0.5 m s^{-1}~~.At CWEX-13,~~. Given the dominant southerly wind conditions~~dominated the campaign. Thus~~, the WINDCUBE 200S scanning lidar can use horizontal (PPI) scans, to observe wakes propagating from the row of four turbines of interest. The horizontal scans were performed at six different elevation angles, giving a range of different vertical positions depending on the distance from the lidar. ~~Elevation~~ Approximately ten minutes were required to collect the series of six elevation tilts; elevation angles varied from 1.5° to 2.8°, which allow measurements at a variety of vertical positions between the bottom and top of the rotor disk of the

Table 2. Description of the 30-min cycle of scanning lidar scans in CWEX-13 field campaign. The characteristic fixed angle refers to the elevation angle for PPI and VAD scans, the azimuth angle for RHI scans.

number of scans	type of scan	characteristic fixed angle	duration of each scan	cumulative time
2	VAD	75°, 60°	132 s	0:00 - 4:24
6	PPI	2.8°, 2.5°, 2.2°, 2.1°, 1.8°, 1.5°	104 s	4:24 - 14:48
3	RHI	160°, 170°, 180°	32 s	14:48 - 16:24
6	PPI	2.8°, 2.5°, 2.2°, 2.1°, 1.8°, 1.5°	104 s	16:24 - 26:48
6	RHI	160°, 170°, 180°, 180°, 170°, 160°	32 s	26:48 - 30:00

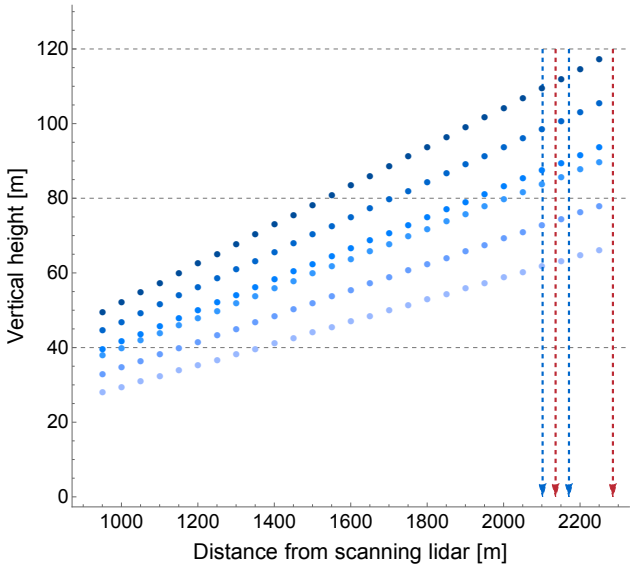

Figure 2. Schematic representation of the position where measurements from PPI scans are available, at ~~6~~ six different elevation angles, as a function of the distance from the scanning lidar. The horizontal dashed lines show the vertical limits of the rotor disk of the turbines and hub height. The position of the ~~4~~ four turbines is represented by the vertical dashed lines, with red lines for outer turbines and blue lines for inner turbines. From the westernmost to the easternmost turbine, the distances from the scanning lidar are 2136 m, 2102 m, 2171 m, and 2286m. The change in elevation between the turbine location and the lidar location (7 m) is taken into account.

turbines, as shown in Figure 2.

We select for a detailed analysis two days (23 and 26 August 2013) displaying wind conditions representative of the typical southerly wind pattern for the site. The first case, 23 August, had predominant southeasterly wind conditions, with relatively low wind speed, which never exceeded 10 m s^{-1} at 220 m AGL. During 23 August 2013, 438 PPI scans were performed, 73 for each of the ~~6~~ six elevation angles. On the other hand, 26 August showed southwesterly wind, which is the most common

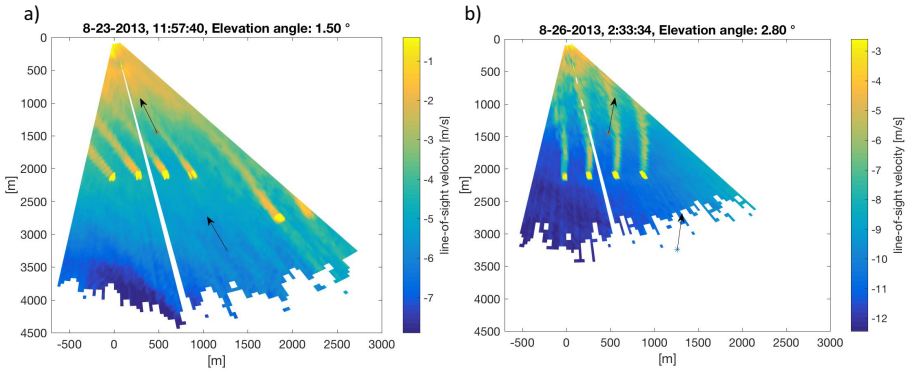

Figure 3. Color maps of line-of-sight velocity measured by the scanning lidar during two PPI scans performed at 11:57 UTC (6:57 LDT) on 23 August 2013 (panel a) and at 02:33 UTC (21:33 LDT) on 26 August 2013 (panel b). The scanning lidar is located in the origin of the coordinate system. The two arrows show wind direction as measured by the profiling lidars WC-1 and WC-2 at 80 m AGL.

situation for the site, with greater wind speed (up to 20 m s^{-1} at 220 m AGL). During 26 August 2013, 576 PPI scans were performed, 96 for each elevation angle. By comparing the results from these two different days, the effect of wind direction on some wake characteristics can be assessed. Figure 3 shows examples of maps of line-of-sight velocity measured by the scanning lidar during two PPI scans performed at night on the selected days. The wind turbine wakes can clearly be detected in terms of reduced wind speed downwind of the four wind turbines.

2.1.2 Surface flux measurements for quantifying atmospheric stability

Several surface flux stations (provided by Iowa State University) were deployed at the CWEX-13 site (orange squares in Figure 1). ~~Measurements from surface flux stations can be used~~ We used measurements from the surface flux station ISU_3 to assess atmospheric stability conditions, with the calculation of Obukhov length L, defined as:

$$L = -\frac{\overline{\theta_v} \cdot u_*^3}{k \cdot g \cdot \overline{w'\theta'_v}} \quad (1)$$

where θ_v is the virtual potential temperature (K), calculated from the sonic anemometer virtual temperature data T_v and the measured pressure p as $\theta_v = T_v \left(\frac{p_0}{p}\right)^{R/c_p}$ with $p_0 = 1000$ hPa, and $R/c_p \approx 0.286$; $k = 0.4$ is the von Kármán constant; $g = 9.81$ m s^{-2} is the acceleration due to gravity; $u_* = (\overline{u'w'}^2 + \overline{v'w'}^2)^{1/4}$ is the friction velocity (m s^{-1}); and $\overline{w'\theta'_v}$ is the kinematic sensible heat flux (W m^{-2}).

Reynolds decomposition for turbulent flows is applied to separate the average and fluctuating parts of the relevant quantities. The average time period used to compute the Reynolds decomposition must be much longer than any turbulence time scale, but much shorter than the time-scale for mean flow unsteadiness. For this purpose, it has been fixed to 30 minutes, a typical time range used to compute turbulent averages for atmospheric boundary layer phenomena (De Franceschi and Zardi, 2003; De Franceschi et al., 2009; Babić et al., 2012).

As to atmospheric stability, we consider neutral atmosphere for $L \leq -500$ m and $L > 500$ m; unstable conditions for ~~$-500 < L \leq 0$~~ -500 m $< L \leq 0$ m; and stable conditions for ~~$0 < L \leq 500$~~ 0 m $< L \leq 500$ m (Muñoz-Esparza et al., 2012).

3 Wake characterization algorithm for multiple wakes

~~Line-of-sight~~ The line-of-sight velocity (u_{LOS}) measured by the WINCDUBE 200S scanning lidar (Figure 4) during the horizontal (PPI) scans can be analyzed to determine wake characteristics and how they evolve in space as the wakes propagate. Aitken et al. (2014a) proposed a wake detection algorithm and applied it to characterize the wake from a single turbine, and later expanded it to treat nacelle-based lidar measurements (Aitken and Lundquist, 2014). Here we expand the same algorithm to characterize wakes from a row of four turbines.

3.1 Data pre-processing

First, a threshold is imposed to the carrier-to-noise ratio (CNR), which represents the strength of the backscattered signal compared to background noise (values closer to 0 dB indicate a stronger signal relative to the noise): all measurements with carrier-to-noise ratio $CNR < -27$ ~~dB~~ dB are discarded from further analysis ~~.~~(Vanderwende et al., 2015). Measurements with a lower CNR often had unrealistically high (> 15 m s^{-1}) values of radial velocity; and this threshold value is comparable with choices in other studies (Cariou et al., 2011; Bastine et al., 2015; Debnath et al., 2016). Moreover, in each scan, line-of-sight velocity data which are not included in the interval $(\mu - 3\hat{\sigma}, \mu + 3\hat{\sigma})$, where μ is the average of the data, are removed from the analysis. The standard deviation $\hat{\sigma}$ is evaluated according to the median absolute deviation (MAD), assuming normally distributed data: $\hat{\sigma} = 1.4826\, MAD$, where $MAD = \text{median}\left(|u_{LOS,i} - \text{median}(u_{LOS})|\right)$. In the remaining part of the wake detection algorithm, measurements will be weighted according to the inverse of the square of the radial wind speed dispersion, which is a measurement of the standard deviation of the back-scattered signal of the lidar and thus an indicator of the uncertainty of values (Vanderwende et al., 2015).

3.2 Wake detection

To implement the wake detection, measurements of line-of-sight velocity u_{LOS} at each range gate in each PPI scan are fitted to two different models: the first is for ambient flow conditions without wakes, the second represents each of the four wakes as a Gaussian function subtracted from uniform ambient flow (Tennekes and Lumley, 1972; Troldborg et al., 2007; Chamorro and Porté-Agel, 2009; Gaumond et al., 2014). Ambient wind speed is modeled with uniform speed u and direction ϕ, as shown in Figure 4. ~~Line-of-sight~~ At a fixed elevation angle, the line-of-sight velocity u_{LOS} can be related to the assumed uniform ambient wind speed u with a simple geometric transformation involving horizontal wind direction ϕ and the lidar azimuth angle α, namely:

$$u_{LOS} = u \cdot \cos(\alpha - \phi) \tag{2}$$

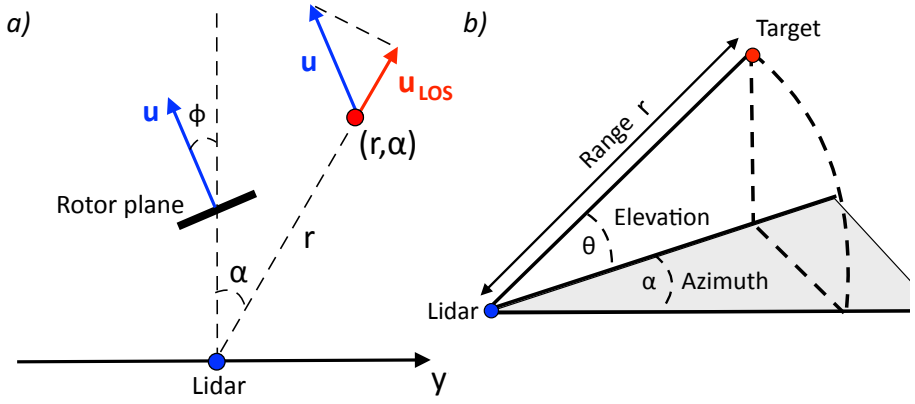

Figure 4. a) Plan view of the coordinate system for scanning lidar PPI scans. b) 3-D sketch of the main geometric quantities relevant in a lidar scan.

where both α and ϕ are > 0 for clockwise rotations from North. The azimuth angle α can be related to the range gate r and the transverse coordinate $y = r \cdot \cos(\theta) \cdot \sin(\alpha)$, yielding:

$$u_{LOS}(y,r) = u \cdot \left(\frac{\sqrt{r^2 - y^2}}{r} \cos\phi + \frac{y}{r} \sin\phi \right) \tag{3}$$

which represents the first model for u_{LOS} applied in the wake detection algorithm. In this case, the ambient flow wind speed u and the ambient wind direction ϕ are the fitting parameters of the model. This "no wake" fit is the same as in Aitken et al. (2014a).

The second implemented model represents each wake from the four turbines in the row as a Gaussian function (Tennekes and Lumley, 1972) subtracted from uniform ambient flow u:

$$u_{LOS}(y,r) = \left\{ u - \sum_{i=1}^{4} a_i \exp\left[-\frac{(y - y_i)^2}{2 s_{wi}^2} \right] \right\} \cdot \left(\frac{\sqrt{r^2 - y^2}}{r} \cos\phi + \frac{y}{r} \sin\phi \right) \tag{4}$$

This second model has 14 fitting parameters: the ambient wind direction ϕ, the ambient wind speed u, the amplitudes of the Gaussian functions (i.e. the wake velocity deficit amplitudes) a_i, the four transverse coordinates of wake centers y_i, and four parameters controlling the widths of the wakes s_{wi}. Note that each of the four wakes is modeled with its own parameters, permitting variable characteristics between the wakes. The amplitude a_i can be 0, for the trivial case of no wake.

Nonlinear regression (least squares) is applied with the two different models specified above. In the fitting procedure, the transverse coordinate y is used as the independent variable, while the measured line-of-sight velocity u_{LOS} is the dependent variable; moreover, the dispersion of measured u_{LOS} is used as weights for the data. In setting the first-guess values for the parameters, physical limits are set: the velocity deficit amplitudes must be ≥ 0 but lower than the uniform ambient flow wind

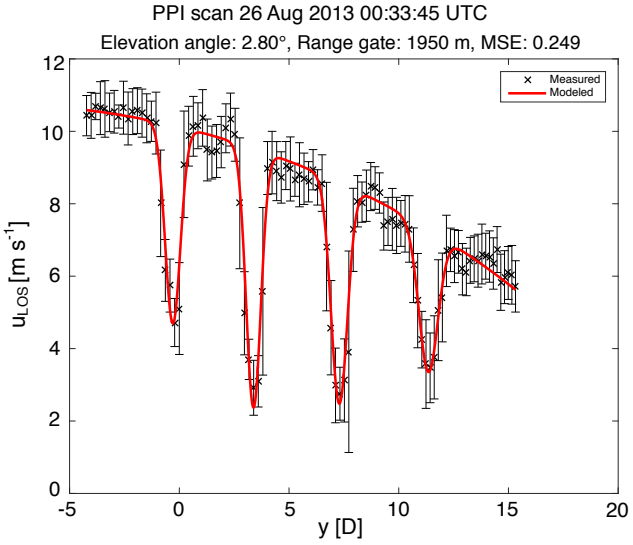

Figure 5. Example of line-of-sight velocity data measured by the scanning lidar at a specific range gate during a PPI scan. Error bars are the dispersion of line-of-sight velocity measurements. The red line represents the fit performed by the wake characterization algorithm.

speed u; the locations of the centers of the wakes must be included in the range of transverse coordinates y in each scan; the width of the wakes must be > 0.

The best estimates for the parameters of the two models are found. An extra sum-of-squares F test is applied to determine if the second model, which is naturally suited to better fit data considering its higher number of parameters, is *significantly* better than first model in fitting the data. A threshold p value is set to 0.05; if the calculated p value is less than this threshold, then the second model is considered capable to *significantly* better represent the data, and thus it is selected (Kleinbaum et al., 2013).

Figure 5 shows an example of line-of-sight velocity measurements at a single range gate in a PPI scan (with error bars representing the dispersion of the measurements). The red continuous line is the fit performed by the wake characterization algorithm.

3.3 Model acceptance criteria

The quality controls implemented in the first steps of the wake detection algorithm (limits to CNR, MAD method to discard outliers, physical limits to the values of the fit parameters) assure a very good quality of the fits, measured in terms of Pearson correlation coefficient and mean squared error. However, some other quality-control steps are applied, to solve possible issues related with the complexity of the expansion of the algorithm to detect multiple wakes.

At the smallest range gates, depending on a given wind direction, not all the four wakes from the studied row of four turbines may be included in the lidar scan because of the limited range of azimuths of each scan. In these situations, the application of the second model, which aims at fitting u_{LOS} with four wakes, may result in the detection of some spurious wakes besides the actual (but less than four) real wakes seen in the PPI scan. These spurious wakes are typically detected where sudden - but

very limited - natural changes in the line-of-sight velocity occur. To solve this false detection, fitted wakes with non-realistic velocity deficits (smaller than half of the minimum velocity deficits of the other wakes detected at the same range gate) and/or widths (smaller than $0.1D$ or bigger than $1/4$ of the whole transverse range) are excluded from the results.

Another issue is related to the possibility for the algorithm to detect wakes with a double-peaked shape - typical of near-wake (Magnusson, 1999), or arising from the interference of an obstacle with the laser beam of the lidar - as two separate wakes. The algorithm detects a double-peaked wake when the transverse positions of the centers of two adjacent wakes are closer than half of the width of the largest wake. When these double-peaked wakes are detected, the algorithm can instead consider a single-peaked wake with a velocity deficit amplitude which is the average of the two detected velocity deficit amplitudes, a wake center located at the average y between the two detected peaks, and a wake width determined adding a half-width ($= 2s_{wi}$) to each external edge of the two detected peaks.

Besides these quality-control steps, the algorithm can re-order the remaining wake parameters, to associate them to the correct physical wake from the considered row of four turbines. This procedure is dependent on wind direction, that determines in which order the four wakes are excluded from the scan area of the lidar at lower range gates.

The wake characteristics database, resulting as output of the application of the wake detection algorithm (which is publicly available at https://github.com/nicolabodini/CWEX13), is then used to study how wake characteristics evolve in 3-dimensional space.

For each detected wake, the velocity deficit is calculated as the ratio between the velocity deficit amplitude a_i and the ambient flow wind speed u (estimated from our algorithm at each performed fit at each range gate and elevation) (Vermeer et al., 2003):

$$VD_i = \frac{u - u_{wake}}{u} \cdot 100 = \frac{a_i}{u} \cdot 100 \tag{5}$$

The wake width has been defined in different ways in the literature; here we calculate it as in Hansen et al. (2012):

$$w_i = 4 \cdot s_{wi} \tag{6}$$

which is equivalent to the 95% confidence interval of the Gaussian velocity deficit profile.

The wake centerline will be studied considering the temporal evolution of the planar coordinates of the center of each wake, i.e. the peak of the velocity deficit.

As final quality-control steps, the ~~median absolute deviation (MAD)~~ MAD method is applied again to discard wake characteristics which do not lie within three standard deviations of the mean characteristic at each range gate for each whole night (Aitken et al., 2014a); moreover, only fits with Pearson correlation coefficient ($corr(u_{LOS}, \hat{u}_{LOS}; g) = cov(u_{LOS}, \hat{u}_{LOS}; g)/\sqrt{cov(u_{LOS}, u_{LOS}; g}$ where g represents the data weights) larger than 0.9 and mean squared error ($MSE = \frac{1}{\sum_{i=1}^{n} g_i} \sum_{i=1}^{n} g_i(\hat{u}_{LOS,i} - u_{LOS,i})^2$) lower than 0.5 are included in the final analysis of the results.

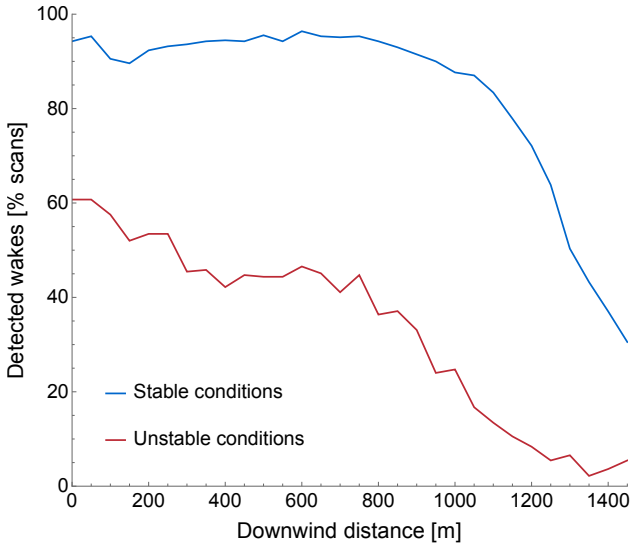

Figure 6. Percentage of wakes which are detected by the characterization algorithm vs downwind distance, for stable and unstable conditions of the atmosphere (neutral conditions were detected only for very short periods, and are not included here). Results from PPI scans performed on 23 and 26 August 2013.

4 Results

Once all the fits are completed, and the wakes fully characterized, it is possible to study how the wake characteristics vary in space for the four studied turbines.

4.1 Frequency of wake detection and atmospheric stability

Atmospheric stability has a major impact (Churchfield et al., 2012; Iungo et al., 2013) on wind turbine wake evolution and wind farm performance: wakes in stable conditions persist for long distances downwind, while during unstable conditions the enhanced turbulent mixing erodes the wakes more quickly.

To get a quantitative measurement of this effect, Figure 6 shows the percentage of scans where wakes were detected by the algorithm, at each range gate, for different stability conditions of the atmosphere (measured in terms of the Obukhov ~~Length)~~ ~~during~~ length) during all the 438/576 scans (at all the considered elevation angles) performed on 23~~and~~ /26 August 2013. The plot clearly shows how wakes can easily be detected in stable conditions, while during unstable conditions the algorithm is not capable of properly detecting wakes at least 40% of the times. Moreover, wakes erode more quickly during unstable conditions, with the degradation becoming more intense approximately at 700 m ($\sim 8.5D$) downwind of the wind turbines, while under stable conditions wakes are detected in most of the scans up to approximately 1000 m ($\sim 12D$) downwind of the turbines.~~The results obtained are comparable for the two considered days: wind direction does not affect this result.~~

All the results presented in the next paragraphs focus on stable conditions of the atmosphere.

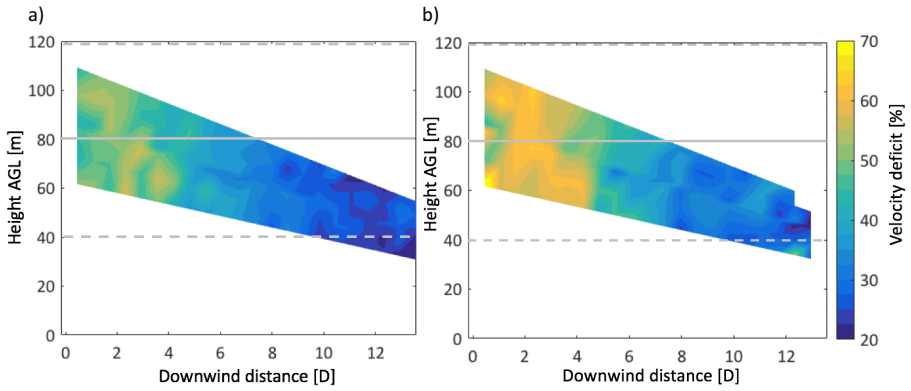

Figure 7. Velocity deficit vs downwind distance, at different vertical positions, for wakes from a) an outer turbine and b) an inner turbine. Gray horizontal dashed lines represent the vertical limits of the rotor disk of the turbines; the horizontal continuous gray line shows the hub height of the turbines. Data collected from 5:31 to 5:42 UTC (from 00:31 to 00:42 LDT), 26 August 2013, from a succession of six PPI scans performed at six different elevation angles.

4.2 Velocity deficit results

Wind speed reduction in the wake region, measured in terms of velocity deficit, is the most distinct wake effect. Figure 7 shows contour plots of velocity deficits for a wake from an outer turbine (panel a) and a wake from an inner turbine (panel b), computed using the results of the wake detection algorithm from PPI scans performed at six different elevation angles from 05:31 to 05:42 UTC (from 00:31 to 00:42 LDT), 26 August 2013. The horizontal axis shows the downwind distance from the turbines, expressed in terms of rotor diameters D, with $D = 80$ m. The plot clearly shows that the velocity deficit decreases with downwind distance, and the wake of the outer turbine exhibits smaller velocity deficits compared to the wake of the inner turbine.

To understand if the results are systematic, Figure 8 shows velocity deficit versus downwind distance from the turbines, calculated from the 276 ~~PPI scans~~ (242) PPI scans, at all the elevation angles, performed during the whole night ~~(stable conditions) -~~ stable conditions - of 26 (23) August 2013. The continuous lines show the median values of velocity deficit, and the shaded area represents the standard deviation of the data. As expected, velocity deficit decreases with downwind distance, since the speed reduction in the wake tends to become smaller due to the entrainment of free-stream surrounding air. The plot also confirms that wakes from outer turbines ~~, shown in red in the plot,~~ (number 1 and number 4), have lower velocity deficits than the wakes from inner turbines (number 2 and number 3), for relatively ~~low downwind distances: for one of the two outer turbines the difference is~~ small downwind distances, with a difference up to 15%~~, while for the other it is of the order of 5%. Comparable results occur with using data from the scans performed during the night of 23 August 2013~~. The presence of outer turbines seems to reduce the effectiveness of lateral entrainment of faster air to recover wind conditions in the inner wake regions of the wind farm. These results are comparable for both the considered nights: different wind directions do not seem to affect ~~these results~~them.

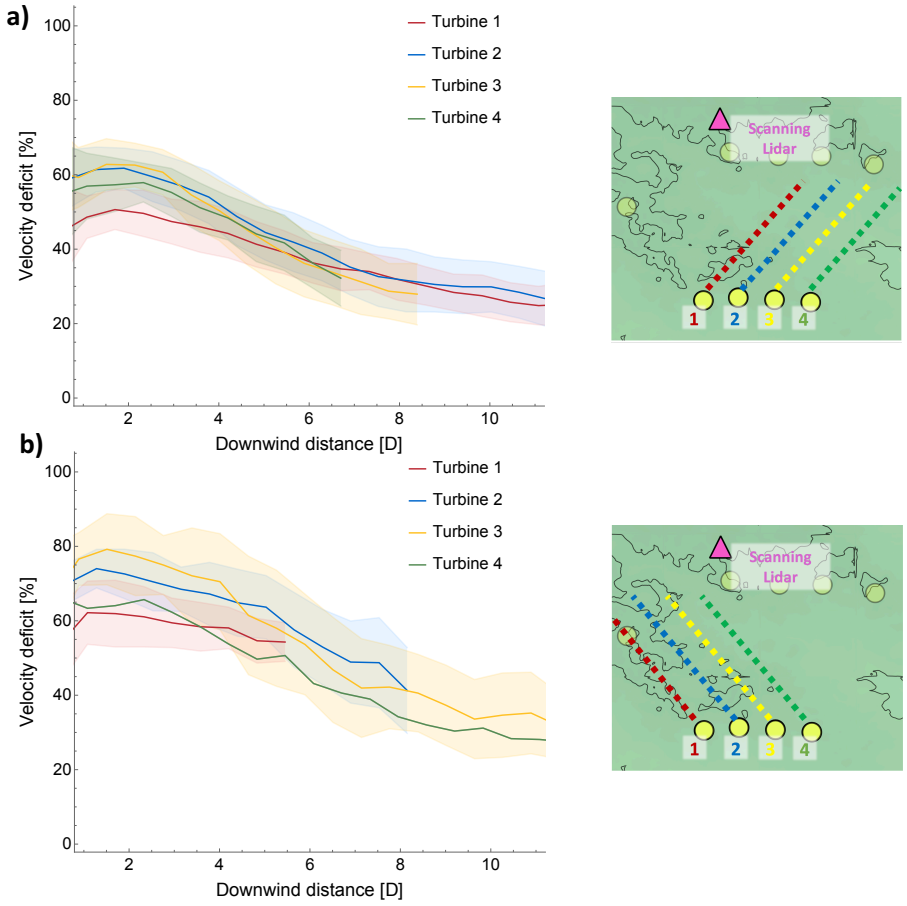

Figure 8. Velocity deficit vs downwind distance, for the four wakes of the studied row of turbines. Continuous lines represent the median values calculated from the ~~276~~ PPI scans performed at all the considered elevation angles during the night (stable conditions) of 26 (panel a) and 23 (panel b) August 2013; shaded areas show ~~the~~ $\pm$ one standard deviation of the data.

4.3 Wake width results

The widths of the wakes also change with downwind distance (expressed in terms of rotor diameters D, Figure 9). Panel a) shows results from the stable conditions of the night of 26 August 2013, while panel b) shows results for the stable conditions of the night of 23 August 2013. In both cases, for all the four turbines, the wake widths increase moving away from the turbine, exceeding 2 D after a downwind distance of 8-10 D.

However, if we focus on the single wakes, we can see how different wind directions (southwesterly during 26 August, south-easterly during 23 August) can affect the ability of the scanning lidar to measure line-of-sight velocity and, thus, detect this characteristic of the wakes. By comparing the two plots in panels a) and b), it is clear that the scanning lidar systematically identifies as the ~~largest~~ widest the wake which, at a given downwind distance, is ~~more~~ the most perpendicular to the laser beam

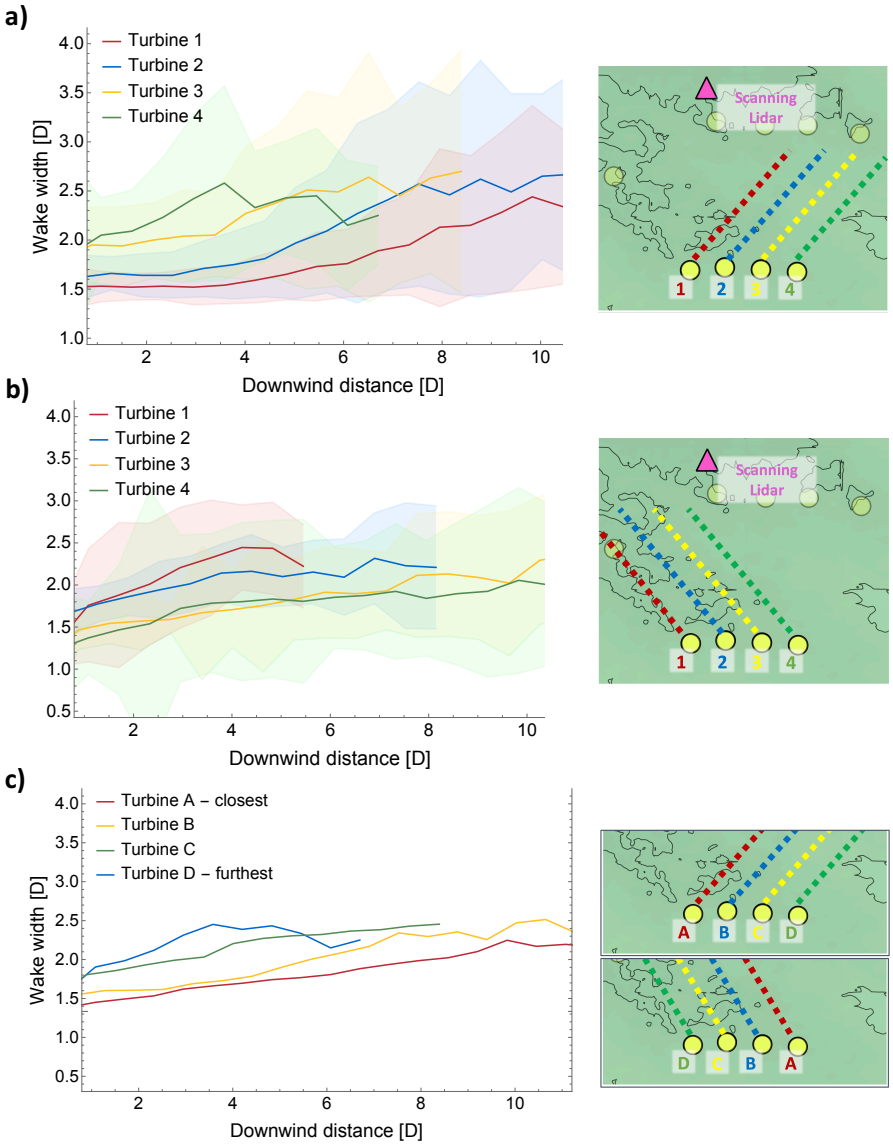

Figure 9. Wake width vs downwind distance from the turbines, for the wakes of the four turbines in the studied row, from PPI scans performed at all the six considered elevation angles. Continuous lines represent median values; shaded areas show ~~the~~ ± one standard deviation of the data. a) Data from the night (stable conditions) of 26 August 2013, with southwesterly wind conditions. b) Data from the night (stable conditions) of 23 August 2013, with southeasterly wind conditions. c) Aggregated plot, average of data from the nights of 26 and 23 August, considering the single turbines with reference to their relative distance from the scanning lidar.

(i.e. the last one the laser beam meets: turbine 4, at the right edge of the row, for southwesterly wind; turbine 1, at the left edge of the row, for southeasterly wind). Then the detected width of the wakes progressively decreases moving to the wakes from adjacent turbines.

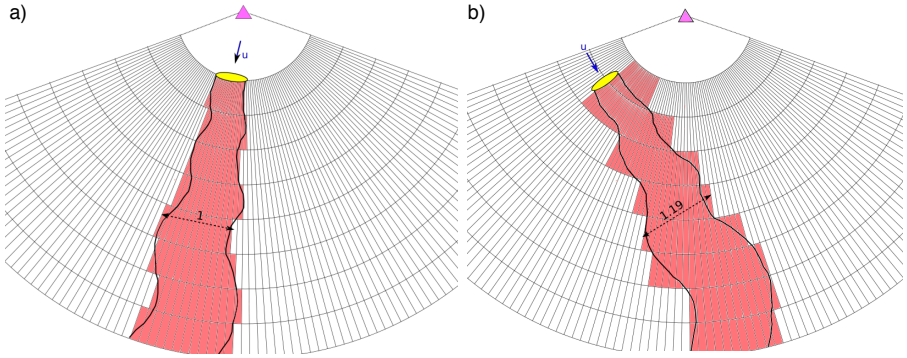

Figure 10. Qualitative sketch of the dependence of detected wake width on the orientation of the coordinate grid used by a scanning lidar (purple triangle) as a function of the wind direction. Panel (a) shows the case of a wake aligned with the line-of-sight from the scanning lidar (wind direction shown by the blue arrow), while panel (b) shows the case of a wake not aligned with the line-of-sight from the lidar. The dashed arrow highlights the difference in the detected wake width for the two cases, at fixed downwind distance from the turbine (yellow ellipse).

Panel c) in Figure 9 aggregates results from 23 and 26 August, and it shows how wake width changes with downwind distance considering the single turbines from the closest to the furthest from the scanning lidar, depending on the particular wind direction, as shown in the right schemes in the panel. The plot confirms the systematic dependence of the detected wake widths on the relative position between the wake and the scanning lidar.

This result is due to the relationship between the viewing angle and the aspect ratio of the lidar retrieval "pixels", which are related to the relatively long range gate (50 m) and relatively narrow azimuthal resolution (0.5°). As qualitatively shown in the schematic of Figure 10, the scanning lidar measures the line-of-sight velocity in narrow pencil-shaped "pixels". With this geometry, if the wind direction - and thus the wake - is aligned with the line-of-sight from the lidar, the wake width can be assessed with high precision due to the high azimuthal resolution in each pencil-shaped area (panel a). However, if the wind direction - and thus the wake - is not aligned with the line-of-sight from the lidar (panel b), then the same wake will be measured as generally wider, since the retrieval of the wake width is now affected by the relatively coarse radial resolution of the lidar coordinate grid. In the schematic diagram shown in Figure 10, at an arbitrary fixed downwind distance from the turbine, the (same) wake would be detected as 19% larger when it is not aligned with the line-of-sight from the scanning lidar. This result becomes more evident when the laser beam is more perpendicular to the wake. This result is due to the aspect ratio of the lidar "pixels," and thus would affect other wake characterization approaches relying on instruments not co-located with the turbine - such as in Banta et al. (2015); Aitken et al. (2014a) - but would not affect nacelle-mounted wake measurements, such as in Bingöl et al. (2010); Aitken and Lundquist (2014) as nacelle-mounted wake measurements are usually aligned with the wake, unless the wake is intentionally yawed (Fleming et al., 2016; Trujillo et al., 2016).

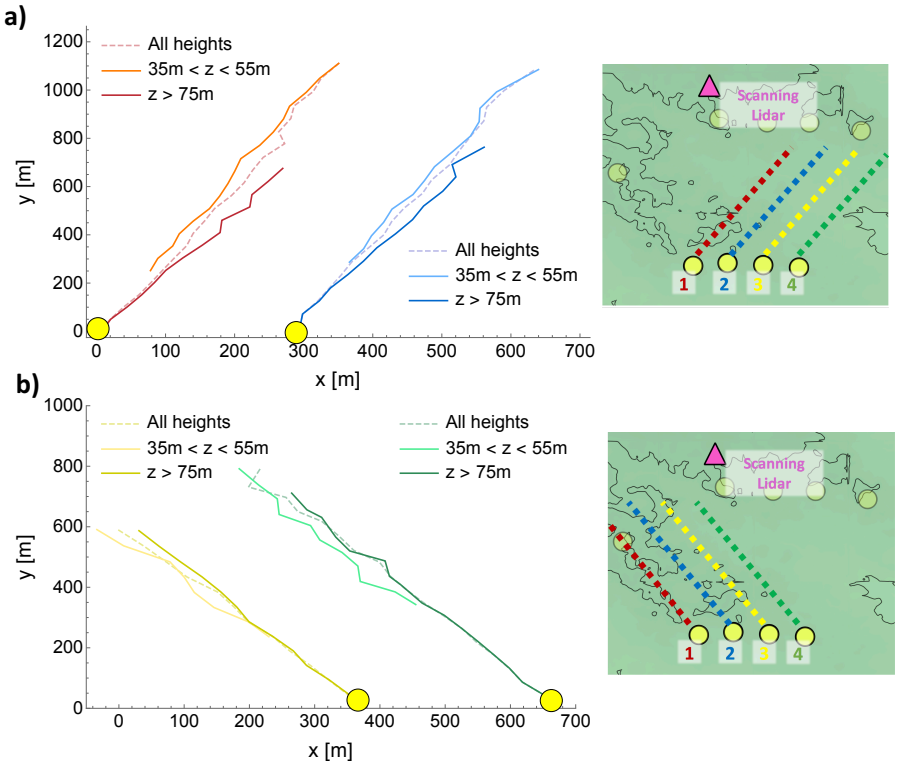

Figure 11. a) Wake centerlines for an outer (on the left) and inner (on the right) turbine, from the PPI scans measurements during the 2:30-3:30 UTC (~~9~~21:~~30-10~~30-22:30 ~~pm~~ LDT) time period, 26 August 2013. b) Wake centerlines for an inner (on the left) and outer (on the right) turbine, data from the 9:30-10:30 UTC (4:30-5:30 ~~am~~ LDT) time period, 23 August 2013. Dashed lines represent the median values of wake centerlines, while the continuous lines show results at different vertical levels: for each wake, light colors refer to measurements between 35 m and 55 m AGL, while darker colors represent data points with a vertical height greater than 75 m. Yellow dots show the position of wind turbines.

4.4 Wake centerline results

PPI scans at multiple elevation angles provide insight into the 3-dimensional structure of wind turbine wakes. Different conditions at different vertical levels have a considerable impact on the wake centerline, i.e. the change of the position of the wake center downwind of the turbine. Figure 11 shows a plot of the median position of the centers for the wakes of the two turbines located at the west edge of the considered row of four turbines, for the 2:30 - 3:30 UTC (~~9:30-10~~21:30-22:30 ~~pm~~ LDT) time period during the night of 26 August 2013 (southwesterly wind, panel a) and for the two turbines located at the east edge of the considered row of four turbines for the 9:30 - 10:30 UTC (4:30-5:30 ~~am~~ LDT) time period during the night of 23 August 2013 (southeasterly wind, panel b). Dashed lines represent the median value for the wake centerlines; continuous lines show the results for data points with different vertical heights: light colors show results for points with a vertical height between ~~35 m and 55 m~~35 m and 55 m, dark colors refer to measurements taken above ~~75 m AGL~~ 75 m AGL (these levels were chosen to

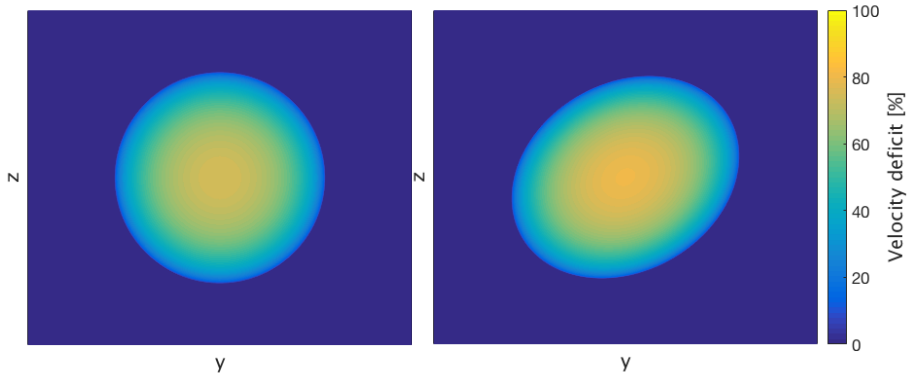

Figure 12. Qualitative cross-stream slices of stream-wise velocity deficit. The perspective is looking downwind. On the left, a graphic representation of the classical Gaussian shape of the magnitude of wake velocity deficit. On the right, an ellipsoid which represents the vertical stretching of the 3-D structure of a turbine wake as a consequence of wind veer.

create bins at low and high heights, compared to the vertical dimension of the turbines, with approximately the same number of vertical positions where the lidar measurements were taken, as shown in Figure 2). A clear change in the position of the wake centers is detected between low and high vertical levels. This stretching is independent of wind direction: the change can be seen for both southwesterly (panel a, 26 August) and southeasterly (panel b, 23 August) wind conditions.

This change of the wake centerline with vertical height causes a stretching of the vertical structure of the wakes: the velocity deficit structure of a turbine wake, whose stream-wise velocity deficit is traditionally considered as a 3-D Gaussian in a cross-stream plan (Figure 12 - a), should instead be represented - when this vertical stretching occurs - by a rotated ellipsoid (Figure 12 - b), as already observed in both field measurements (Högström et al., 1988; Magnusson and Smedman, 1994) and large-eddy simulations ~~(?Vollmer et al., 2016a)~~(Lundquist et al., 2015; Vollmer et al., 2016b).

4.4.1 Relationship between ambient veer and wake centerline

The vertical stretching of wake structure occurs because of the wind veer, the clockwise change of wind direction with height that occurs in strongly stable conditions, like those of 23 and 26 August 2013. To get a deeper insight on the relationship between ambient wind veer and vertical changes of the wake centerlines, we analyze several 30-minute periods (each corresponding to two subsequent sequences of six PPI scans at the six different elevation angles) during the nights of 23 August 2013 (southeasterly wind) and 26 August 2013 (southwesterly wind). For each considered time frame, the wind veer is calculated as the average difference between the wind direction at ~~100 m and 40 m~~100 m and 40 m, as measured by the vertical profiling lidar located to measure upwind conditions (WC-1 in Figure 1). The two vertical heights are chosen as representative of the two different vertical levels considered when assessing the changes of wake centerlines (35 m $< z <$ 55 m and $z >$ 75 m). Moreover, the wake centerlines at different vertical levels have been fitted with straight lines, and the angle between the lines which approximate the wake centerlines at 35 m $< z <$ 55 m and $z >$ 75 m is calculated and then considered as the angular difference between the wake centerlines at different vertical levels. Figure 13 shows how angular difference between

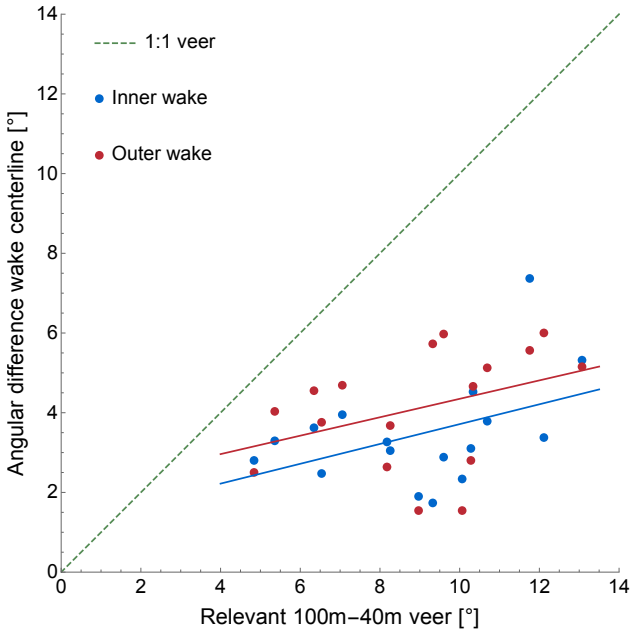

Figure 13. Angular difference between wake centerlines at different vertical heights (35 m $< z < 55$ m and $z > 75$ m) *vs* wind veer between 100 m and 40 m. Data for an inner and an outer wake in the considered row of ~~4~~ four turbines, for several 30-minutes time frames during the nights of 23 and 26 August 2013. Continuous lines are the linear regressions from the data (red best-fit: $2.04 + 0.23x$, blue best-fit: $1.23 + 0.25x$), for the outer and the inner wake. Dashed line highlights the not-reached equality between ambient veer and wake centerlines angular difference.

wake centerlines at different vertical levels compares to ambient wind veer between 100 m and 40 m, for all the available time frames during the nights of 23 and 26 August 2013, for wakes from an inner and an outer turbine in the considered row. The results show that, although the angular change in the wake centerline at different vertical levels is systematically detected, the wind veer is always much larger than the actual angular difference between the wake centerlines at the different vertical levels: the change of the positions of the wake centers is related to, but not completely determined by, the wind veer. Moreover, as suggested by the linear regression fits, wakes from outer turbines often present a larger angular difference in wake centerlines compared to wakes from inner turbines, ~~as shown by the linear regression fits~~though with variability for different veer values that motivates further study.

A possible physical explanation for this phenomenon can be detected in the interaction between wake rotation due to rotating blades and wind veer. The blades of the wind turbines in CWEX-13 wind farm rotate clockwise and so the downwind wakes rotates counter-clockwise (Burton et al., 2001).The wake can thus be considered as a sort of plume with its own momentum and rotation, which interacts with the ambient veer, that in turns tends to rotate the wake in the opposite direction (in the Northern hemisphere), thus causing a reduction in the global wake vertical stretching than would be present if only the ambient veer

affected the wake. Inner wakes seem to be less subject to the effect of ambient wind veer, as if the presence of outer turbines reduces the ability of ambient wind characteristics to reach and impact inner regions of the wind farms.

5 Conclusions

Wakes from a row of four turbines have been characterized using line-of-sight wind speed measurements from PPI scans performed by a scanning lidar. Data were collected in late summer 2013 during the CWEX-13 field campaign (Lundquist et al., 2014), in a wind farm in a flat region in central Iowa. The wake characterization algorithm proposed by Aitken et al. (2014a) has been extended to assess wakes from multiple turbines.

Wakes erode quickly during unstable conditions of the atmosphere, and they can in fact be detected here primarily in stable conditions in this dataset. The velocity deficit in the wakes decreases with downwind distance from the turbines, and it is lower for wakes from outer turbines in the studied row. The width of the wakes increases with downwind distance, with systematic differences in the ability of the scanning lidar to detect the width of the wake according to the component of the direction the wakes perpendicular to the direction of laser beam of the scanning lidar. Wake centerlines change at different vertical levels as a consequence of the ambient wind veer, causing a stretching of the vertical structure of the wakes. Although the field measurements of Högström et al. (1988); Magnusson and Smedman (1994) demonstrated that turbine wakes stretch into ellipses during stable conditions, for the first time we have quantified the effect of ambient wind veer on the stretching of wakes. In fact, the angular change in the wake centerlines at different heights is systematically much lower (a half or less) than the wind veer registered at the same heights. Moreover, this angular change of the wake centerlines at different vertical levels is found to be usually greater for wakes from outer turbines. This wake stretching, due to wind veer, is not only seen in these field measurements but also emerges in the stably-stratified simulations of Aitken et al. (2014b); Bhaganagar and Debnath (2015); Lundquist et al. (2015); Vollmer et al. (2016b); Abkar et al. (2016). As more three-dimensional measurements of wakes become available due to the use of scanning lidar and scanning radar, a more solid representation of wind turbine wakes can be assessed.

These results can become critically important to assess and improve large-eddy simulations of wakes as well as to suggest improvements to mesoscale parametrizations (Fitch et al., 2012, 2013; Jiménez et al., 2015; Lee and Lundquist, 2017) to account for subgridscale wake interactions. Moreover, wind energy companies can also benefit from our results in trying to enhance the quality of low-order wake models currently used for wind resource assessment, wind farm layout optimization and wind farm control techiniques, with the final goal of an improvement of wind energy production efficiency.

6 Code availability

The Matlab code of the wake characterization algorithm is publicly available at https://github.com/nicolabodini/CWEX13.

7 Data availability

CWEX-13 data will be publicly-available at the Dept. of Energy Atmosphere to electrons archive at https://a2e.energy.gov/projects.

Acknowledgements. This work was partially supported by the National Renewable Energy Laboratory under APUP UGA-0-41026-22 and by the National Science Foundation grant BCS-1413980 (Coupled Human Natural Systems). Nicola Bodini was partiallly supported by a grant from the University of Trento for a visit to the University of Colorado Boulder in summer 2016.

References

Abkar, M. and Porté-Agel, F.: Influence of atmospheric stability on wind-turbine wakes: A large-eddy simulation study, Physics of Fluids, 27, 035 104, 2015.

Abkar, M., Sharifi, A., and Porté-Agel, F.: Large-eddy simulation of the diurnal variation of wake flows in a finite-size wind farm, in: Journal of Physics: Conference Series, vol. 625, p. 012031, IOP Publishing, 2015.

Abkar, M., Sharifi, A., and Porté-Agel, F.: Wake flow in a wind farm during a diurnal cycle, Journal of Turbulence, 17, 420–441, doi:10.1080/14685248.2015.1127379, 2016.

Aitken, M. L. and Lundquist, J. K.: Utility-scale wind turbine wake characterization using nacelle-based long-range scanning lidar, Journal of Atmospheric and Oceanic Technology, 31, 1529–1539, doi:10.1175/JTECH-D-13-00218.1, 2014.

Aitken, M. L., Banta, R. M., Pichugina, Y. L., and Lundquist, J. K.: Quantifying wind turbine wake characteristics from scanning remote sensor data, Journal of Atmospheric and Oceanic Technology, 31, 765–787, doi:10.1175/JTECH-D-13-00104.1, 2014a.

Aitken, M. L., Kosović, B., Mirocha, J. D., and Lundquist, J. K.: Large eddy simulation of wind turbine wake dynamics in the stable boundary layer using the Weather Research and Forecasting Model, Journal of Renewable and Sustainable Energy, 6, 033 137, doi:10.1063/1.4885111, 2014b.

Andersen, S. J., Sørensen, J. N., Ivanell, S., and Mikkelsen, R. F.: Comparison of engineering wake models with CFD simulations, in: Journal of physics: Conference series, vol. 524, p. 012161, IOP Publishing, 2014.

Aubrun, S., Garcia, E. T., Boquet, M., Coupiac, O., and Girard, N.: Wind turbine wake tracking and its correlations with wind turbine monitoring sensors. Preliminary results, in: Journal of Physics: Conference Series, vol. 753, p. 032003, IOP Publishing, 2016.

Babić, K., Bencetić Klaić, Z., and Večenaj, Ž.: Determining a turbulence averaging time scale by Fourier analysis for the nocturnal boundary layer, Geofizika, 29, 35–51, 2012.

Banta, R. M., Pichugina, Y. L., Brewer, W. A., Lundquist, J. K., Kelley, N. D., Sandberg, S. P., Alvarez II, R. J., Hardesty, R. M., and Weickmann, A. M.: 3D volumetric analysis of wind turbine wake properties in the atmosphere using high-resolution Doppler lidar, Journal of Atmospheric and Oceanic Technology, 32, 904–914, 2015.

Barthelmie, R., Larsen, G., Frandsen, S., Folkerts, L., Rados, K., Pryor, S., Lange, B., and Schepers, G.: Comparison of wake model simulations with offshore wind turbine wake profiles measured by sodar, Journal of atmospheric and oceanic technology, 23, 888–901, 2006.

Barthelmie, R. J., Pryor, S., Frandsen, S. T., Hansen, K. S., Schepers, J., Rados, K., Schlez, W., Neubert, A., Jensen, L., and Neckelmann, S.: Quantifying the impact of wind turbine wakes on power output at offshore wind farms, Journal of Atmospheric and Oceanic Technology, 27, 1302–1317, 2010.

Barthelmie, R. J., Hansen, K. S., and Pryor, S. C.: Meteorological controls on wind turbine wakes, Proceedings of the IEEE, 101, 1010–1019, 2013.

Bastine, D., Wächter, M., Peinke, J., Trabucchi, D., and Kühn, M.: Characterizing Wake Turbulence with Staring Lidar Measurements, J. Phys.: Conf. Ser., 625, 012 006, doi:10.1088/1742-6596/625/1/012006, 2015.

Bhaganagar, K. and Debnath, M.: The effects of mean atmospheric forcings of the stable atmospheric boundary layer on wind turbine wake, Journal of Renewable and Sustainable Energy, 7, 013 124, doi:10.1063/1.4907687, 2015.

Bingöl, F., Mann, J., and Larsen, G. C.: Light detection and ranging measurements of wake dynamics part I: one-dimensional scanning, Wind Energy, 13, 51–61, doi:10.1002/we.352, 2010.

Brower, M.: Wind resource assessment: a practical guide to developing a wind project, John Wiley & Sons, 2012.

Burton, T., Sharpe, D., Jenkins, N., and Bossanyi, E.: Wind energy handbook, John Wiley & Sons, 2001.

Cariou, J.-P., Sauvage, L., Thobois, L., Gorju, G., Machta, M., Lea, G., and Duboué, M.: Long range scanning pulsed Coherent Lidar for real time wind monitoring in the Planetary Boundary Layer, in: 16th Coherent Laser Radar Conference 2011, pp. 148–152, 2011.

Chamorro, L. P. and Porté-Agel, F.: A Wind-Tunnel Investigation of Wind-Turbine Wakes: Boundary-Layer Turbulence Effects, Boundary-Layer Meteorology, 132, 129–149, doi:10.1007/s10546-009-9380-8, 2009.

Chowdhury, S., Zhang, J., Messac, A., and Castillo, L.: Unrestricted wind farm layout optimization (UWFLO): Investigating key factors influencing the maximum power generation, Renewable Energy, 38, 16–30, 2012.

Churchfield, M. J., Lee, S., Michalakes, J., and Moriarty, P. J.: A numerical study of the effects of atmospheric and wake turbulence on wind turbine dynamics, Journal of turbulence, p. N14, 2012.

Clifton, A., Smith, A., and Fields, M.: Wind Plant Preconstruction Energy Estimates: Current Practice and Opportunities, Tech. rep., NREL (National Renewable Energy Laboratory (NREL), Golden, CO (United States)), http://www.nrel.gov/docs/fy16osti/64735.pdf, 2016.

Clive, P. J., Dinwoodie, I., and Quail, F.: Direct measurement of wind turbine wakes using remote sensing, Proc. EWEA 2011, 2011.

Crespo, A., Hernandez, J., and Frandsen, S.: Survey of modelling methods for wind turbine wakes and wind farms, Wind energy, 2, 1–24, 1999.

De Franceschi, M. and Zardi, D.: Evaluation of cut-off frequency and correction of filter-induced phase lag and attenuation in eddy covariance analysis of turbulence data, Boundary-layer meteorology, 108, 289–303, 2003.

De Franceschi, M., Zardi, D., Tagliazucca, M., and Tampieri, F.: Analysis of second-order moments in surface layer turbulence in an Alpine valley, Quarterly Journal of the Royal Meteorological Society, 135, 1750–1765, 2009.

Debnath, M., Iungo, G. V., Brewer, W. A., Choukulkar, A., Delgado, R., Gunter, S., Lundquist, J. K., Schroeder, J. L., Wilczak, J. M., and Wolfe, D.: Assessment of virtual towers performed with scanning wind lidars and Ka-band radars during the XPIA experiment, Atmospheric Measurement Techniques Discussions, 2016, 1–19, doi:10.5194/amt-2016-325, http://www.atmos-meas-tech-discuss.net/amt-2016-325/, 2016.

Dörenkämper, M., Witha, B., Steinfeld, G., Heinemann, D., and Kühn, M.: The impact of stable atmospheric boundary layers on wind-turbine wakes within offshore wind farms, Journal of Wind Engineering and Industrial Aerodynamics, 144, 146–153, doi:10.1016/j.jweia.2014.12.011, 2015.

Elkinton, C. N., Manwell, J. F., and McGowan, J. G.: Offshore wind farm layout optimization (OWFLO) project: Preliminary results, University of Massachusetts, 2006.

Fitch, A. C., Olson, J. B., Lundquist, J. K., Dudhia, J., Gupta, A. K., Michalakes, J., and Barstad, I.: Local and Mesoscale Impacts of Wind Farms as Parameterized in a Mesoscale NWP Model, Monthly Weather Review, 140, 3017–3038, doi:10.1175/MWR-D-11-00352.1, 2012.

Fitch, A. C., Olson, J. B., and Lundquist, J. K.: Parameterization of Wind Farms in Climate Models, Journal of Climate, 26, 6439–6458, doi:10.1175/JCLI-D-12-00376.1, 2013.

Fleming, P. A., Gebraad, P. M., Lee, S., van Wingerden, J.-W., Johnson, K., Churchfield, M., Michalakes, J., Spalart, P., and Moriarty, P.: Evaluating techniques for redirecting turbine wakes using SOWFA, Renewable Energy, 70, 211–218, 2014.

Fleming, P. A., Ning, A., Gebraad, P. M. O., and Dykes, K.: Wind plant system engineering through optimization of layout and yaw control, Wind Energ., 19, 329–344, doi:10.1002/we.1836, 2016.

Gaumond, M., Réthoré, P.-E., Ott, S., Pena, A., Bechmann, A., and Hansen, K. S.: Evaluation of the wind direction uncertainty and its impact on wake modeling at the Horns Rev offshore wind farm, Wind Energy, 17, 1169–1178, 2014.

Gebraad, P., Teeuwisse, F., Wingerden, J., Fleming, P. A., Ruben, S., Marden, J., and Pao, L.: Wind plant power optimization through yaw control using a parametric model for wake effects—a CFD simulation study, Wind Energy, 19, 95–114, 2016.

Hansen, K. S., Barthelmie, R. J., Jensen, L. E., and Sommer, A.: The impact of turbulence intensity and atmospheric stability on power deficits due to wind turbine wakes at Horns Rev wind farm, Wind Energy, 15, 183–196, 2012.

Hirth, B. D. and Schroeder, J. L.: Documenting Wind Speed and Power Deficits behind a Utility-Scale Wind Turbine, Journal of Applied Meteorology and Climatology, 52, 39–46, doi:10.1175/JAMC-D-12-0145.1, 2013.

Hirth, B. D., Schroeder, J. L., Gunter, W. S., and Guynes, J. G.: Measuring a utility-scale turbine wake using the TTUKa mobile research radars, Journal of Atmospheric and Oceanic Technology, 29, 765–771, 2012.

Hirth, B. D., Schroeder, J. L., Gunter, W. S., and Guynes, J. G.: Coupling Doppler radar-derived wind maps with operational turbine data to document wind farm complex flows, Wind Energy, 18, 529–540, 2015a.

Hirth, B. D., Schroeder, J. L., Irons, Z., and Walter, K.: Dual-Doppler measurements of a wind ramp event at an Oklahoma wind plant, Wind Energy, 2015b.

Högström, U., Asimakopoulos, D., Kambezidis, H., Helmis, C., and Smedman, A.: A field study of the wake behind a 2 MW wind turbine, Atmospheric Environment (1967), 22, 803–820, 1988.

Iungo, G. V., Wu, Y.-T., and Porté-Agel, F.: Field Measurements of Wind Turbine Wakes with Lidars, Journal of Atmospheric and Oceanic Technology, 30, 274–287, doi:10.1175/JTECH-D-12-00051.1, 2013.

Jensen, N. O.: A note on wind generator interaction, 1983.

Jensen, N. O., Petersen, E. L., and Troen, I.: Extrapolation of Mean Wind Statistics with Special Regard to Wind Energy Applications., Tech. rep., 1984.

Jiménez, P. A., Navarro, J., Palomares, A. M., and Dudhia, J.: Mesoscale modeling of offshore wind turbine wakes at the wind farm resolving scale: a composite-based analysis with the Weather Research and Forecasting model over Horns Rev, Wind Energ., 18, 559–566, doi:10.1002/we.1708, 2015.

Käsler, Y., Rahm, S., Simmet, R., and Kühn, M.: Wake measurements of a multi-MW wind turbine with coherent long-range pulsed Doppler wind lidar, Journal of Atmospheric and Oceanic Technology, 27, 1529–1532, 2010.

Katic, I., Højstrup, J., and Jensen, N. O.: A simple model for cluster efficiency, in: European Wind Energy Association Conference and Exhibition, pp. 407–410, 1986.

Kleinbaum, D. G., Kupper, L. L., Nizam, A., and Rosenberg, E. S.: Applied regression analysis and other multivariable methods, Nelson Education, 2013.

Kumer, V.-M., Reuder, J., Svardal, B., Sætre, C., and Eecen, P.: Characterisation of single wind turbine wakes with static and scanning WINTWEX-W LiDAR data, Energy Procedia, 80, 245–254, 2015.

Landberg, L.: Meteorology for Wind Energy: An Introduction, John Wiley & Sons, 2015.

Lee, J. C.-Y. and Lundquist, J.: Observing and Simulating Wind Turbine Wakes during the Evening Transition, Boundary-Layer Meteorology, in review, 2017.

Lundquist, J. K., Takle, E. S., Boquet, M., Kosović, B., Rhodes, M. E., Rajewski, D., Doorenbos, R., Irvin, S., Aitken, M. L., Friedrich, K., et al.: Lidar observations of interacting wind turbine wakes in an onshore wind farm, in: EWEA meeting proceedings, 2014.

Lundquist, J. K., Churchfield, M. J., Lee, S., and Clifton, A.: Quantifying error of lidar and sodar Doppler beam swinging measurements of wind turbine wakes using computational fluid dynamics, Atmos. Meas. Tech., 8, 907–920, doi:10.5194/amt-8-907-2015, 2015.

Machefaux, E., Larsen, G. C., Koblitz, T., Troldborg, N., Kelly, M. C., Chougule, A., Hansen, K. S., and Rodrigo, J. S.: An experimental and numerical study of the atmospheric stability impact on wind turbine wakes, Wind Energy, 2015.

Magnusson, M.: Near-wake behaviour of wind turbines, Journal of Wind Engineering and Industrial Aerodynamics, 80, 147–167, 1999.

Magnusson, M. and Smedman, A.: Influence of atmospheric stability on wind turbine wakes, Wind Engineering, 18, 139–152, 1994.

Mirocha, J. D., Kosovic, B., Aitken, M. L., and Lundquist, J. K.: Implementation of a generalized actuator disk wind turbine model into the weather research and forecasting model for large-eddy simulation applications, Journal of Renewable and Sustainable Energy, 6, 013 104, doi:10.1063/1.4861061, 2014.

Mirocha, J. D., Rajewski, D. A., Marjanovic, N., Lundquist, J. K., Kosović, B., Draxl, C., and Churchfield, M. J.: Investigating wind turbine impacts on near-wake flow using profiling lidar data and large-eddy simulations with an actuator disk model, Journal of Renewable and Sustainable Energy, 7, 043 143, 2015.

Muñoz-Esparza, D., Cañadillas, B., Neumann, T., and van Beeck, J.: Turbulent fluxes, stability and shear in the offshore environment: Mesoscale modelling and field observations at FINO1, Journal of Renewable and Sustainable Energy, 4, 063 136, doi:10.1063/1.4769201, 2012.

Neustadter, H. and Spera, D.: Method for evaluating wind turbine wake effects on wind farm performance, Journal of Solar Energy Engineering, 107, 240, 1985.

Nygaard, N. G.: Wakes in very large wind farms and the effect of neighbouring wind farms, in: Journal of Physics: Conference Series, vol. 524, p. 012162, IOP Publishing, 2014.

Rajewski, D. A., Takle, E. S., Lundquist, J. K., Oncley, S., Prueger, J. H., Horst, T. W., Rhodes, M. E., Pfeiffer, R., Hatfield, J. L., Spoth, K. K., and Doorenbos, R. K.: CROP WIND ENERGY EXPERIMENT (CWEX): Observations of Surface-Layer, Boundary Layer, and Mesoscale Interactions with a Wind Farm, Bulletin of the American Meteorological Society, 94, 655–672, http://0-search.proquest.com.libraries.colorado.edu/docview/1368160232/abstract/2AD773836C1B4F73PQ/1, 2013.

Rhodes, M. E. and Lundquist, J. K.: The Effect of Wind-Turbine Wakes on Summertime US Midwest Atmospheric Wind Profiles as Observed with Ground-Based Doppler Lidar, Boundary-Layer Meteorology, 149, 85–103, doi:10.1007/s10546-013-9834-x, 2013.

Samorani, M.: The wind farm layout optimization problem, in: Handbook of Wind Power Systems, pp. 21–38, Springer, 2013.

Sathe, A. and Mann, J.: A review of turbulence measurements using ground-based wind lidars, Atmospheric Measurement Techniques, 6, 3147–3167, doi:10.5194/amt-6-3147-2013, http://www.atmos-meas-tech.net/6/3147/2013/, 2013.

Sathe, A., Mann, J., Barlas, T., Bierbooms, W., and van Bussel, G.: Influence of atmospheric stability on wind turbine loads: Atmospheric stability and loads, Wind Energy, 16, 1013–1032, doi:10.1002/we.1528, http://doi.wiley.com/10.1002/we.1528, 2013.

Takle, E. S., Rajewski, D. A., Lundquist, J. K., Jr, W. A. G., and Sharma, A.: Measurements in support of wind farm simulations and power forecasts: The Crop/Wind-energy Experiments (CWEX), J. Phys.: Conf. Ser., 524, 012 174, doi:10.1088/1742-6596/524/1/012174, 2014.

Tennekes, H. and Lumley, J. L.: A first course in turbulence, MIT press, 1972.

Troldborg, N., Sørensen, J. N., and Mikkelsen, R.: Actuator line simulation of wake of wind turbine operating in turbulent inflow, in: Journal of physics: conference series, vol. 75, p. 012063, IOP Publishing, 2007.

Trujillo, J.-J., Bingöl, F., Larsen, G. C., Mann, J., and Kühn, M.: Light detection and ranging measurements of wake dynamics. Part II: two-dimensional scanning, Wind Energy, 14, 61–75, 2011.

Trujillo, J. J., Seifert, J. K., Würth, I., Schlipf, D., and Kühn, M.: Full-field assessment of wind turbine near-wake deviation in relation to yaw misalignment, Wind Energy Science, 1, 41, 2016.

van Dooren, M. F., Trabucchi, D., and Kühn, M.: A Methodology for the Reconstruction of 2D Horizontal Wind Fields of Wind Turbine Wakes Based on Dual-Doppler Lidar Measurements, Remote Sensing, 8, 809, 2016.

Vanderwende, B. J. and Lundquist, J. K.: The modification of wind turbine performance by statistically distinct atmospheric regimes, Environmental Research Letters, 7, 034 035, doi:10.1088/1748-9326/7/3/034035, 2012.

Vanderwende, B. J., Lundquist, J. K., Rhodes, M. E., Takle, E. S., and Irvin, S. L.: Observing and Simulating the Summertime Low-Level Jet in Central Iowa, Monthly Weather Review, 143, 2319–2336, doi:10.1175/MWR-D-14-00325.1, 2015.

Vermeer, L., Sørensen, J. N., and Crespo, A.: Wind turbine wake aerodynamics, Progress in aerospace sciences, 39, 467–510, 2003.

Vollmer, L., Steinfeld, G., Heinemann, D., and Kühn, M.: Estimating the wake deflection downstream of a wind turbine in different atmospheric stabilities: an LES study, Wind Energy Science, 1, 129–141, doi:10.5194/wes-1-129-2016, http://www.wind-energ-sci.net/1/129/2016/, 2016a.

Vollmer, L., Steinfeld, G., Heinemann, D., and Kühn, M.: Estimating the wake deflection downstream of a wind turbine in different atmospheric stabilities: An LES study, Wind Energy Science, in open discussion, doi:doi:10.5194/wes-2016-4, 2016b.

Wang, H. and Barthelmie, R.: Wind turbine wake detection with a single Doppler wind lidar, in: Journal of Physics: Conference Series, vol. 625, p. 012017, IOP Publishing, 2015.

Wharton, S. and Lundquist, J. K.: Atmospheric stability affects wind turbine power collection, Environmental Research Letters, 7, 014 005, doi:10.1088/1748-9326/7/1/014005, 2012.